Organic carbon stocks, quality and prediction in permafrost-affected forest soils in North Canada

Marcus Schiedung, Severin-Luca Bellè, Avni Malhotra, Samuel Abiven

Catena 213 (2022) 106194

Contents lists available at ScienceDirect

Catena

journal homepage: www.elsevier.com/locate/catena

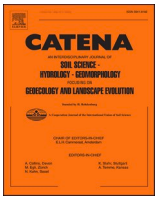

Organic carbon stocks, quality and prediction in permafrost-affected forest soils in North Canada

Marcus Schiedung [a], Severin-Luca Bellè [a], Avni Malhotra [a], Samuel Abiven [a,b,c,*]

[a] Department of Geography, University of Zurich, Winterthurerstrasse 190, 8057 Zurich, Switzerland
[b] Laboratoire de Géologie, CNRS – École normale supérieure, PSL University, Institut Pierre Simon Laplace, Rue Lhomond 24, 75005 Paris, France
[c] CEREEP-Ecotron Ile De France, ENS, CNRS, PSL University, Chemin de busseau 11, 77140 Saint-Pierre-lès-Nemours, France

ARTICLE INFO

Keywords:
Boreal forest soils
Permafrost
Soil organic carbon
High latitude
DRIFT
PLSR predictive modelling

ABSTRACT

High-latitude soils store a large amount of the global soil organic carbon (SOC). The SOC stocks in mineral soils under different permafrost conditions, however, are underrepresented in global carbon databases. We sampled mineral forest soils under continuous and discontinuous to sporadic permafrost conditions on the Canadian Boreal and Taiga Plain. We determined the SOC stocks in the upper 60 cm of 94 soil pits across eleven sites (5–9 pits per site) and SOC quality using ^{13}C isotopic signatures, C:N ratios and composition of aliphatic/aromatic and cellulose/lignin-like compounds obtained from mid-infrared spectra analyses. Lastly, we evaluated the prediction of SOC stocks in these soils using mid-infrared spectra and partial least square regression modelling (PLSR). The SOC stocks were on average four times higher in soils under continuous permafrost conditions (93.7–203.8 Mg SOC ha^{-1} in 0–45 cm) compared to soils under discontinuous to sporadic permafrost conditions (26.7–60.2 Mg SOC ha^{-1} in 0–60 cm). In addition, the SOC stocks were larger at moist and wet locations compared to dryer locations and varied significantly between sites, stressing the importance of small-scale geomorphic differences in controlling SOC in boreal mineral forest soils. Continuous permafrost SOC had a lower degree of decomposition compared to soils under discontinuous and sporadic permafrost. This indicates a potentially large proportion of SOC in boreal mineral soils to be vulnerable to warming associate increases in decomposition. The combination of mid-infrared with PLSR was suitable to predict the SOC stocks ($R^2 > 0.8$) with an average uncertainty of 14–23%, which was less than the observed spatial variability of the field replicates (29–41%). Mid-infrared spectroscopy can thus offer an alternative to fill SOC data gaps of high latitude mineral forest soils and reduce uncertainties originating from the limited number of currently available SOC observations of Canadian boreal mineral forest soils.

1. Introduction

High latitude soils in the Northern Hemisphere store approximately 1100–1500 Pg organic carbon in the upper three meters (Jobbágy and Jackson, 2000). This corresponds to 30–40% of the global soil organic carbon (SOC), despite high latitude regions covering only 15% of the Earth's surface (Köchy et al., 2015; McGuire et al., 2009). The largest proportion (63–88%) of the total SOC is potentially located in permanently frozen soil depth of organic and mineral permafrost soils. Peatlands and wetlands are known as a major carbon (C) reservoir of the high latitudes (Hugelius et al., 2020). However, it is estimated that nearly 70% of the total SOC of the Boreal and Tundra biomes is located in mineral soils (Jackson et al., 2017), which have received less attention so far.

Northern high latitude regions are experiencing rapid climate warming with projected increases of up to 8 °C during the next decades (Erdozain et al., 2019; IPCC, 2013). The extent of permafrost is already decreasing and 40% of the global permafrost is predicted to thaw within the next decades even with a limited global mean annual temperature increase of 2 °C (Biskaborn et al., 2019; Camill, 2005; Chadburn et al., 2017). Due to altered hydrology and plant productivity, enhanced microbial SOC decomposition and ultimately increased greenhouse gas production, permafrost thaw could further accelerate global climate change (Chen et al., 2021; Schädel et al., 2016; Schuur et al., 2015; Turetsky et al., 2020). In the contexts of high latitude soils, climate warming and permafrost thaw, the present and future quantity and

* Corresponding author at: Department of Geography, University of Zurich, Winterthurerstrasse 190, 8057 Zurich, Switzerland.
E-mail address: samuel.abiven@geo.uzh.ch (S. Abiven).

https://doi.org/10.1016/j.catena.2022.106194
Received 27 August 2021; Received in revised form 24 February 2022; Accepted 1 March 2022
Available online 12 March 2022

quality of SOC in mineral boreal forest soils is uncertain.

Northern SOC data of mineral soils are poorly represented in global databases of soil carbon, particularly from carbon-rich boreal forest soils (Batjes et al., 2019; Malhotra et al., 2019). The limited data and understanding of C dynamics in boreal mineral forest soils constrains the precision of predictive earth system models and estimation of the C-related feedbacks with climate change (Hugelius et al., 2014). In particular, SOC content and stock data are scarce for Canadian soils, where the boreal forest covers more than 300 million hectares (Brandt et al., 2013; Kurz et al., 2013). Most of the available observations are located in the more populated southern regions of Canada and therefore, the lack of observations is even larger in regions of the more remote northern parts. Shaw et al. (2018) recently published a database on upland forest soils in Canada, which indicates that of the total available 3500 observations, only 5% (approx. 180 observations) stem from regions above 60° north. So far, only a few studies exist that quantify SOC stocks in North Canadian boreal mineral soils (e.g.(Hossain et al., 2007; Tarnocai and Bockheim, 2011; Tarnocai et al., 2009), study its quality (e.g. Laganière et al., 2013; Matamala et al., 2019) or estimate SOC stocks indirectly from, for example, soil type data (Shaw et al., 2008). This lack of data and understanding of SOC in northern mineral soils limits our ability to predict northern soil carbon and permafrost thaw feedbacks (Dai et al., 2019; Luo et al., 2016; Poggio et al., 2021).

Boreal forest mineral soils have high variability in SOC dynamics and unique features related to permafrost and cryoturbation. Around two-thirds of the boreal forest soils are on continuous permafrost with a rough gradient to sporadic and discontinuous permafrost conditions towards the south (Gruber, 2012; Helbig et al., 2016). Around 35% of the Canadian soils are Cryosols of which approx. 84% are mineral soils and 16% are organic Cryosols, the latter can be classified as peat- and wetlands (Tarnocai and Bockheim, 2011). Mineral Cyrosols are estimated to store 490–610 Mg SOC ha^{-1} in the upper meter, which would represent around 55 Gt C, while non-cryoturbated soils are estimated to store less C with 120–170 Mg SOC ha^{-1} in the same depth (Tarnocai and Bockheim, 2011). Cryoturbation is an important process of the C cycle in boreal soils and results in a translocation and mixing of SOC to greater soil depth (Bockheim, 2007; Ping et al., 2015). The extent and depth of cryoturbation and SOC translocation depends on factors such as drainage, soil texture (e.g. favored by high silt content) and freeze–thaw cycles (Ping et al., 2015; Walker et al., 2004). Consequently, cryoturbation is controlled by small-scale geomorphic differences along the landscape, which also influence the composition of vegetation and the initial input of organic matter to the soil (Walker et al., 2004). However, given the lack of data for these regions, our understanding of how SOC stocks and its quality and composition relates to geographical distribution, spatial heterogeneity and permafrost conditions is limited.

Mid-infrared spectroscopy offers an opportunity for compound-specific analyses of SOC and to differentiate, for example, aliphatic and aromatic or lignin- and cellulose-like compounds (Cotrufo et al., 2016; Laub et al., 2020; Ofiti et al., 2021; Soucémarianadin et al., 2019). It can be used to determine the quality and chemical characteristics of SOC. Recently, mid-infrared analyses in combination with statistical spectra analysis are gaining attention because it offers a possibility for a time- and cost-efficient determination of soil properties (e.g. pH and texture) and SOC contents (Dangal et al., 2019; Ludwig et al., 2016). In general, mid-infrared analyses are semi-quantitative but can be used in a chemometric approach to predict soil properties and SOC contents in combination with, for example, partial least square regression (PLSR) or machine learning algorithms. Several studies have shown that SOC contents could be well predicted for large datasets across the United States (Sanderman et al., 2020) and Europe (Nocita et al., 2014), but also the prediction of SOC fractions was possible (Sanderman et al., 2021; Ramírez et al., 2021).

A great advantage would be to predict volumetric SOC contents and hence directly estimate SOC stocks (quantity of SOC per area for a given depth) from mid-infrared spectra, which reduces the fieldwork efforts to estimate accurate bulk densities (Bellon-Maurel and McBratney, 2011). This is particularly challenging in high latitude soils due to logistical and sampling constraints in frozen soils and remote dense forests. Due to the cold environmental conditions, SOC in boreal soils is suggested to be little processed (Calderón et al., 2017; Tinti et al., 2015). Therefore, mid-infrared analyses based on the abundance of single components and functional groups of the SOC are promising for evaluating and predicting SOC quality and contents. Matamala et al. (2017) reported a good prediction of SOC contents and its decomposition state in organic layers and mineral soils of 27 sites in high latitude regions of Alaska, Canada and Iceland. To our knowledge, no study has reported a prediction of volumetric SOC contents and stocks of high latitude soils using mid-infrared analysis.

Here, we determined SOC stocks and its quality in Canadian boreal forest mineral soils using 94 profiles (0–60 cm depth) to address the following questions: 1) Does continuous permafrost promote the accumulation of SOC in forest soils along the whole profile? 2) Which factors control SOC stocks and quality in continuous, discontinuous to sporadic permafrost soils and at different landscape positions? 3) Can the SOC stocks be predicted sufficiently with mid-infrared spectroscopy to provide a rapid alternative to fill missing data from high latitude mineral forest soils?

We selected forest soils under continuous and discontinuous to sporadic permafrost located in the Boreal and Taiga Plain of Alberta and the Northwest Territories, Canada. Additionally, we sampled different landscape positions (e.g. elevated plateau, slope and flat lowland) to identify controlling factors, such as soil and environmental properties, of the SOC stocks. Beside the quantification of SOC, we assessed its quality using $\delta^{13}C$ values and C:N ratios as well as analyzing mid-infrared spectra obtained by diffuse reflectance infrared Fourier transformed (DRIFT) spectroscopy. Lastly, we used our dataset, composed of nearly 300 measured SOC contents, bulk densities and spectra, for predictive PLSR modelling.

2. Material and methods

2.1. Study sites and soils

We sampled at eleven sites within the Boreal and Taiga Plain, which can be divided in soils under continuous permafrost (hereafter northern sites) and discontinuous to sporadic permafrost conditions (hereafter southern sites) (Fig. 1, Table 1). The site descriptions below are based on field observations and reports of the National Ecological Framework of Canada (Agriculture and Agri-Food Canada, 2013) and the ecological regions of the Northwest Territories – Taiga Plain report (Ecosystem Classification Group, 2007).

Five northern sampling sites were located near the town Inuvik (N1-N5) in the northern and permafrost dominated Taiga Plain with a high subarctic ecoclimate (mean annual temperature: −9.5 °C and mean annual precipitation: 200–300 mm). Four sites (N1-N4) were located in the Great Bear Lake Plain. A landscape gradient (N2-N4; approx. 580 m in length, 50–90 m a.s.l. and maximum slope of 15°) was sampled on the Campbell Hills facing north towards the Campbell Lake. The Campbell Hills are characterized by Pleistocene glacial till and colluvial deposits on Devonian limestone and dolomites (Campbell Uplift). The flat regions of the Great Bear Lake Plain (N1) are characterized by undulating fine textured glacial and outwash deposits on Cretaceous shale and Devonian limestone. The last sampling site (N5) was located on a hill (105 m a.s.l., Inuvik weather station) in the Mackenzie Delta ecozone. The Great Bear Lake Plain and the Mackenzie Delta ecozone are covered by approximately 50% peatland and the forests are dominated by open white (*Picea glauca*) and black spruce (*Picea mariana*) and tamarack (*Larix laricina*) stands with a ground cover of dwarf birch (*Betula nana*), dwarf willow (*Salix herbacea*), ericaceous shrubs (*Ericaceae*), cotton grass (*Eriophorum vaginatum*) and lichen. Alaska paper birch (*Betula neoalaskana*) occurs in moist colluvial sites and in succession zones. All soils in the north were

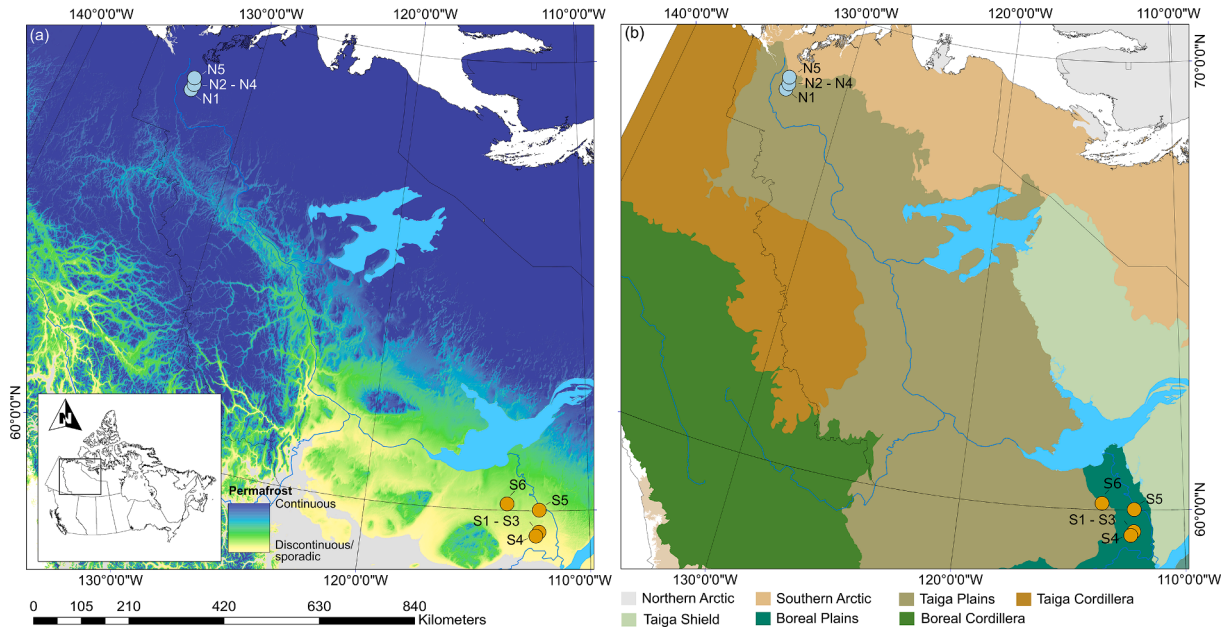

Fig. 1. Locations of northern (N1-N5) and southern (S1-S6) sites with permafrost distribution (a) and ecozones of Canada (b). The permafrost distribution is based on Gruber (2012) and ecozones on the Ecosystem Classification Group (2007).

Table 1
Site and soil characteristics of soils at northern (N1-N5) and southern (S1-S6) locations with coordinates (latitude and longitude), landscape position, elevation, active layer as observed in sampling depth, texture, soil type, dominant forest stand species and site moisture class.

Site	Latitude Longitude	Landscape position	Elevation (m a.s.l.)	Active layer[a] (cm)	Texture[b] (%)			Soil type[c]	Dominant forest stand species	Moisture class[d]
					Sand	Silt	Clay			
N1	68°02'32.0''N 113°29'17.9''W	Lowland	75	20–30	23	50	27	Turbic Cryosol	*Picea mariana, Betula neoalaskana*	Mesic to subhygric (3)
N2	68°10'07.5''N 133°26'03.2''W	Bottom	50	20–30	19	52	29	Turbic Cryosol	*Picea mariana, Betula neoalaskana*	Mesic to subhygric (3)
N3	68°10'11.7''N 133°25'43.4''W	Slope	65	15–40	26	47	27	Turbic Cryosol	*Picea mariana, Populus balsamifera*	Mesic (2)
N4	68°10'20.5''N 133°25'26.4''W	Top	90	20–60	12	52	36	Cambic Cryosol	*Picea mariana, Populus balsamifera, Salix herbacea*	Subxeric (1)
N5	68°19'01.0''N 133°31'57.2''W	Elevated plateau	105	10–40	23	54	23	Skeletic Cryosol	*Picea mariana, Populus balsamifera, Salix herbacea*	Subxeric to mesic (2)
S1	59°31'31.9''N 112°13'17.7''W	Bottom	270	>60	81	15	4	Stagnic Regosol	*Picea mariana*	Mesic (2)
S2	59°31'29.5''N 112°13'17.6''W	Slope	275	>60	75	19	6	Haplic Regosol	*Picea mariana, Pinus banksiana*	Subxeric to mesic (2)
S3	59°31'27.5''N 112°13'20.7''W	Top	290	>60	78	17	5	Haplic Cambisol	*Picea mariana, Pinus banksiana, Populus balsamifera*	Subxeric to mesic (2)
S4	59°26'24.6''N 112°21'12.2''W	Flat Plateau	315	>60	71	20	9	Haplic Cambisol	*Picea mariana, Populus balsamifera*	Subxeric to mesic (2)
S5	60°01'02.2''N 112°12'18.8''W	Dune/ river bank	180	>60	83	12	5	Haplic Regosol	*Pinus banksiana,*	Xeric (1)
S6	60°08'38.2''N 113°38'55.5''W	Lowland	270	>60	24	66	10	Leptic Luvisol	*Pinus banksiana,*	Xeric (1)

[a] observed within the maximum sampling depth of 60 cm in summer 2019 as a range of all pits.
[b] as average of all depths with clay (<0.002 mm), silt (0.002–0.05 mm) and sand (0.05–2 mm). See Tab. S1 for all depth.
[c] according to World Reference Base (FAO, 2014)
[d] classified according to Johnstone et al. (2008) and summarized as (1) dry, (2) moist and (3) wet.

characterized as Cryosols and the active layer varied between 10 and >60 cm (Table 1) with polygon structures at N4 and N5.

All southern sites (S1-S6) were located in regions with discontinuous to sporadic permafrost and characterized by sub-humid mid-boreal ecoclimate (mean annual temperature: −2°C and mean annual precipitation 300–400 mm) in the southern Northwest Territories and in northern Alberta. We did not observe any frozen soil in the upper 60 cm of the soils sampled for this study. Five sample locations (S1-S5) were located in the Boral Plain of the Slave River Lowlands with sandy undulated alluvial and partly eolian deposits on Paleozoic carbonate formations. Approximately 50% of the surface of the ecozone is covered with peatlands. Three sites (S1-S3) were located on a landscape gradient (approx. 170 m length, 270–290 m a.s.l. and maximum slope of 12°) exposed to the north towards a sinkhole lake, the Pine Lake in the Wood Buffalo National Park. The site S4 was located at the edge of a degraded peatland and the southernmost site in this study under a succession forest. The site S5 was located on a periglacial dune west of the town of Fort Smith. The last site in the southern sample region (S6), was located

in the Hay River Lowlands at the transition from Boreal to Taiga Plain and is dominated by clayey lacustrine and glacial till on Cretaceous shale with widely shallow soils (e.g. <30 cm). This ecozone has a peatland surface cover of 30%. At all southern sites, the forest is dominated by closed stands of jack pine (*Pinus banksiana)*, white (*Picea glauca*) and black spruce (*Picea mariana*), trembling aspen (*Populus tremuloides*) and balsam poplar (*Populus balsamifera*), and white birches (*Betula papyrifera*) in successions and moist areas. The soils in the southern region were classified as Gleysols, Regosols and Cambisols (Table 1).

Based on the reconstruction of the deglaciation and retreat of the Laurentide Ice Sheet using radiocarbon-based ice margin chronology, Dalton et al. (2020) reported ice-free conditions around 12 ka cal. BP for the northern sites and around 10 ka cal. BP for the southern sites of this study. However, the southern sites have been covered by the Glacial Lake McConnell after the retreat. It is estimated that the lake divided into the today present Great Slave Lake and Lake Athabasca between 5.0 and 8.3 ka cal. BP with the isostatic rebound and elevation of the land surface (Smith, 1994).

Moisture classes of each site, in six levels from xeric to subhygric, were determined by considering topographic drainage, permafrost and soil texture following the key presented by Johnstone et al. (2008). The moisture classes were summarized in: (1) dry: xeric or suxeric. (2) moist: subxeric-mesic or mesic and (3) wet: mesic-subhygric to subhygric (Table 1).

2.2. Soil sampling

All soils were sampled in July and August 2019. At each of the eleven sample locations, a sample grid of 30x30 m was implemented and sampled in a raster, resulting in nine sample points per location. It was only possible to establish eight sample points at S1 and five at S6 due to logistical reasons. At each sample point, soil pits were excavated by hand using a spade to a depth of 60 cm. From each pit, four depth increments of the mineral soil (0–15 cm, 15–30 cm, 30–45 cm and 45–60 cm) were sampled with stainless-steel soil cores (5 cm diameter and 12 cm length taken centered of the increment), which were driven in by hand. Three soil cores were composited per increment. Undisturbed soil cores (100 cm^3) were taken in each pit for each depth increment to estimate bulk densities.

Organic layers were sampled at the centered location of the sampling grid and the total layer contained litter and humified organic matter. At all other sample points, the thickness of the organic layers was measured and then carefully removed prior to mineral soil sampling. The sampling was restricted to less than 60 cm due to shallow soils and too high rock contents for some sample points in the south. At site S6 only the upper 0–15 cm were sampled due to continuous rock in >15 cm depth. Continuous permafrost at the northern sites restricted the sampling to an average depth of 30 cm. However, deeper sampling was conducted if possible. Unless stated otherwise, all data are presented as averages of three to nine depth increments of each sample site. The number of samples per depth increment and per site are given in Table S1. In total, 289 samples were taken from 94 pits. A full soil profile characterization was conducted at the centered pit of the sampling grids for each sampling site.

2.3. Sample preparation

The bulk density at each sampled depth from each pit was estimated by determining the gravimetric water content of the undisturbed and field moist samples, by drying at 105 °C until constant weight. Afterwards, the samples were sieved to <2 mm to determine the mass of coarse rock and root fragments and to obtain the fine soil bulk density.

The composited samples from the pits were air-dried and sieved to <8 mm for homogenization. To reduce the sample mass (1–2 kg per sample were taken in the field), an aliquot was dried at 40 °C and sieved to <2 mm. An aliquot of this was milled for further analysis.

All samples with a pH > 6 were decarbonized using a HCl fumigation approach presented by (Walthert et al., 2010). In brief, 50 µl of 1% HCl were added to the samples in silver cups (5 × 9 mm) and exposed for eight hours to 37% HCl vapor. Afterwards, the samples were dried for four days under vacuum. The shift in $\delta^{13}C$ to more negative values was examined in order to evaluate an effective carbonate removal. The decarbonatization concerned only samples of the sites S1-S4 (see Table S1 for all pH values). The remaining southern and all northern sites were free of inorganic carbon. All total carbon, inorganic carbon and SOC contents are presented in Table S1.

We observed a shift to highly negative $\delta^{13}C$ values (>31‰) for samples deeper than 15 cm at the sites S4 and deeper than 30 cm at site S1, S2 and S3. In these depths, all sites showed low SOC contents (<1%) and thus the fumigation may have influenced the isotopic composition of the little available SOC. It is reported that the acid fumigation has no effect on the stable isotopic composition of SOC in temperate soils used in Walthert et al. (2010). The removal of inorganic carbon by acid treatment, however, can alter SOC and change the isotopic composition (Bisutti et al., 2004). After several tests and modifications, we still obtained $\delta^{13}C$ of >31‰ and removed corresponding samples from the interpretation of the isotopic SOC composition.

The organic layers were dried at 40 °C and homogenized in a large bowl to mix the less degraded litter with the humified organic matter. Around 20% of the total weight was randomly sampled and further homogenized by hand. Approximately 10% of this mass was milled for further analysis, providing a representative measurement of the whole organic layer.

2.4. Soil analyses

The total carbon, total organic carbon and $\delta^{13}C$, relative to the international Vienna Pee Dee Belemnite (VPDB) standard, of all milled samples from soils and organic layers were measured using a dry combustion module cavity ring-down spectroscopy system (Picarro, Santa Clara, USA). The total nitrogen of soil samples was measured with the DUMAS method according to ISO 13878:1998. The total nitrogen of the organic layers was measured using an elemental analyzer-isotope ratio mass spectrometer (EA-IRMS; Flash 2000-HT Plus, linked by Conflo IV to Delta V Plus isotope ratio mass spectrometer, Thermo Fisher Scientific, Bremen, Germany).

For each sample site, one composite for each depth increment was generated by weight for the following analyses. The texture was determined by sedimentation and pipette method after removal of organic matter by H_2O_2 according to ISO 11277:2009. The texture classes were classified as clay (<0.002 mm), silt (0.002–0.05 mm) and sand (0.05–2 mm). The effective cation exchange capacity (CEC_{eff}) was determined by hexamminecobalt trichloride extraction according to ISO 23470:2018. The pH was measured in 0.01 M $CaCl_2$ using a 1:2.5 soil-solution ratio after shaking and settling for 1 h (Carter and Gregorich, 2008) using a glass-electrode (914 pH/Conductometer, Metrohm, Herisau, Switzerland). The elemental composition was determined by X-ray fluorescence analysis (Xepos, Spector Analytical Instruments, Kleve, Germany) using an international soil reference material (NCS DC 73319). All soil parameters are presented in the supplement (Table S1).

2.5. Soil organic carbon stock calculation

Our sampling approach provided a bulk density estimation for each field replicate of the SOC content. Accordingly, the SOC stocks were calculated as:

$$SOCstock = SOC_{fine} * BD_{fine} * d \quad (1)$$

where SOC_{fine} is the SOC content [g g^{-1}] in the fine soil (<2 mm), d is the increment depth (15 cm) and BD_{fine} [g cm^{-3}] is the bulk density of the fine soil calculated as:

$$BD_{fine} = \frac{m_{sample} - m_{rock\ fragments} - m_{plant\ fragments}}{V_{sample} - \frac{m_{rock\ fragments}}{\rho_{rock\ fragments}} - \frac{m_{plant\ fragments}}{\rho_{plant\ fragments}}} \quad (2)$$

where m_{sample} is the total mass of sample [g], $m_{rockfragments}$ and $m_{plantfragments}$ are the masses of rock and plant fragments >2 mm [g], respectively, V_{sample} is the sample volume (100 cm^{-3}) and $\rho_{rockfragments}$ and $\rho_{plantfragments}$ are the assumed densities of rock and plant fragments of 2.65 g cm^{-3} and 1.0 g cm^{-3}, respectively. All stocks are cumulated for 0–15, 0–30, 0–45 and 0–60 cm depth for each sample point per sampling site and expressed in [Mg ha^{-1}]. All BD_{fine} are presented with depth in the supplement (Fig. S1). To calculate the C stored in the organic layers, the thickness at each individual sample point was considered but the C content was obtained only from the center pit. The organic layer bulk density was estimated as 0.15 g cm^{-3}, which was obtained from a dataset presented by Shaw et al. (2018), including >2500 data points of Canadian boreal upland forest soils (average of 0.15 ± 0.04 g cm^{-3}).

2.6. Mid-infrared spectroscopy and peak analysis

The milled soil and organic layer samples were used to determine mid-infrared spectra by using DRIFT spectroscopy (TENSOR 27 spectrophotometer, Bruker, Fällanden, Switzerland) at wavelengths from 4000 to 400 cm^{-1} (average of 64 scans per sample at 4 cm^{-1} resolution), using KBr for background correction. After baseline correction and correction for CO_2-interferences, peaks of maximal absorbance were identified for qualitative comparison. Peaks corresponding to cellulose- (band at 1245 cm^{-1}; range of 1247–1240 cm^{-1}) and lignin- (band at 1508 cm^{-1}; range of 1512–1504 cm^{-1}) like compounds as well as aliphatic (band at 2930 cm^{-1}; range of 2990–2915 cm^{-1}) to aromatic (band at 1630 cm^{-1}; range of 1660–1590 cm^{-1}) compounds were considered (Cotrufo et al., 2016; Laub et al., 2020; Matamala et al., 2019; Yeasmin et al., 2017). To identify differences in the SOC composition as a result of organic matter input composition or its degree of decomposition, cellulose:lignin and aliphatic:aromatic maximal absorbance ratios were calculated.

2.7. Partial least squared regression predictive analysis

The PLSR prediction analysis was computed for the northern and southern sites separately. Pre-analysis indicated a clustering of the prediction scores related to the large differences in SOC content and stocks between northern and southern sites. All spectra of each depth were considered, which resulted in 115 and 169 spectra for northern and southern sites, respectively. Only one spectrum in the north and four spectra in the south were excluded due to high SOC contents (>10% SOC). To reach normal distribution, all SOC stocks were log-transformed.

To determine the optimum number of components, Monte Carlo resampling was applied with 100 repetitions and using a four-segment cross validation as an adapted approach from Kvalheim et al. (2018). In order to avoid overparameterization, the maximum number of components was evaluated by considering the median and standard deviation of the root mean squared error of prediction (RMSE) and the Akaike criterium (AIC) of the resampled predictions, which was calculated as:

$$AIC = N\log(RMSE) \times 2m \quad (3)$$

where N is the number of included spectra (samples) and m the number of components (Li et al., 2002).

The minimum RMSE and AIC for the SOC stock prediction was identified with six and eight components for the northern and southern sites, respectively. Student's t-tests were used if AIC values were similar and the lower number of components was considered when differences were not significant (see Fig. S6 and S7).

The SOC stocks were eventually estimated by using a leave-one-out validation, including all spectra and using the previous determined optimal number of components. All PLSR predictions were performed using the *pls* package in R Studio (Mevik and Wehrens, 2007). Beside comparing the RMSE, we further conducted an absolute and relative uncertainty analysis of predicted values in relation to the measured SOC contents and stocks (Fig. S10 and S11).

2.8. Statistics

Analysis of variances (ANOVA) was used to test significant differences of cumulated SOC stocks in 0–15, 0–30, 0–45 and 0–60 cm soil depth between all sites and within sample sites from the northern and southern sample locations. The ANOVA was also used to determine differences of SOC stocks and DRIFT peak ratios between moisture classes. To compute p-values, general linear hypothesis and multiple comparison with post-hoc-test (Tukey) on a 95% pairwise confidence level and multiplicity Bonferroni adjustment was used by using the *multcomp* package (Hothorn et al., 2021). Prior to the ANOVA, homogeneity of variances was tested with a Levene's test. Due to variance heterogeneity, the SOC stocks were log-transformed when all sites (southern and northern locations) were tested. All analyses were done with R Studio (Version 1.3.1073, R Core Team (2021)). All data is shown as means of the field replicates and standard errors of the mean (SE) are presented.

3. Results and discussion

3.1. SOC stocks and contents under continuous and discontinuous permafrost conditions

3.1.1. Mineral soil SOC stocks and contents

The SOC stocks of soils under continuous permafrost from the northern locations were on average 4 ± 2 (up to 10) times higher compared to the southern locations (Fig. 2). Our findings are in line with previous observations, that mineral soils affected by cryoturbation store up to 70% more SOC than soils without cryoturbation (Bockheim, 2007; Kaiser et al., 2007; Tarnocai and Bockheim, 2011), while our findings indicate much larger differences. Only the lowest SOC northern site (N4) was comparable to the highest SOC southern sites (S1, S3, and S4).

The northern SOC stocks ranged between 93.7 and 203.8 Mg SOC ha^{-1} (based only on the upper 0–45 cm; all sites n ≥ 3 pits; Fig. 2 a). Among northern sites, SOC stocks were highest in the lowland and flat landscape positions (N1 and N2); lowest at elevated sites (N4 and N5) and intermediate at the slope location (N3). When taking the limited number of samples below 45 cm into consideration (due to frozen soil in >45 cm), the lowland and flat sites had even higher SOC stocks (N2 = 272.2 ± 24.5 Mg SOC ha^{-1} and N1 = 247.1 Mg SOC ha^{-1} for the whole profile; 0–60 cm depth).

Large proportions of the total SOC were in deeper soil depth at the northern permafrost sites. At these sites, the SOC contents ranged between 2.3 and 6.4% in 0–15 cm and decreased only slightly for the sites in the lowlands (N1 and N2), but remained >2.0% until 60 cm depth (Fig. 3a). For the more elevated sites (N3-N5), the SOC contents decreased with depth down to 1.6% at 60 cm. Our ranges compare well to literature reported values for two soil pits in the vicinity of our sites. A Turbic Cryosol, with 1.1–4.5% SOC similar to our sites N1 and N2, and a Static Cryosol (Canadian soil classification) with 1.5–3.0% SOC similar to our site N4 and N5 (Shaw et al., 2018). The SOC depth distribution indicates that the upper 0–15 cm contributed to 49–57% of the total SOC stocks in 0–45 cm at the elevated sites (N4 and N5) and the site at the slope (N4). At the two lowland sites (N1 and N2), around 54–70% of the whole SOC stocks were located in depth below 15 cm. This indicates that SOC translocation through cryoturbation leads to large stocks of permafrost mineral soils (Bockheim, 2007; Ping et al., 2015).

Our two lowland sites (N1 and N2) are located in similar landforms with shallow active layer depths, a high silt content >50% (Table 1) and high SOC contents throughout the whole soil profiles (>2%, Fig. 3). It is

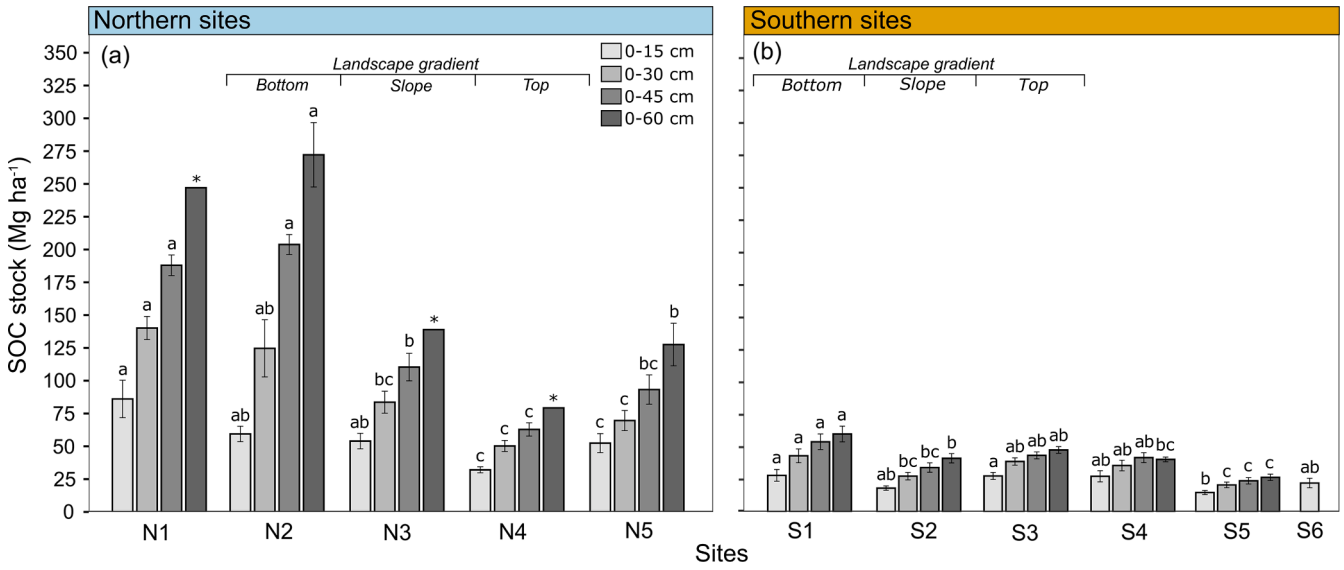

Fig. 2. Total SOC stocks for northern (a) and southern (b) sites in 0–15, 0–30, 0–45 and 0–60 cm depth. Significant differences ($p < 0.05$) of each group in each depth between the sites is indicated with letters. The asterisk indicates if number of sample points was $n < 3$ and only one pit was sampled (see Table S1 for number of samples per depth).

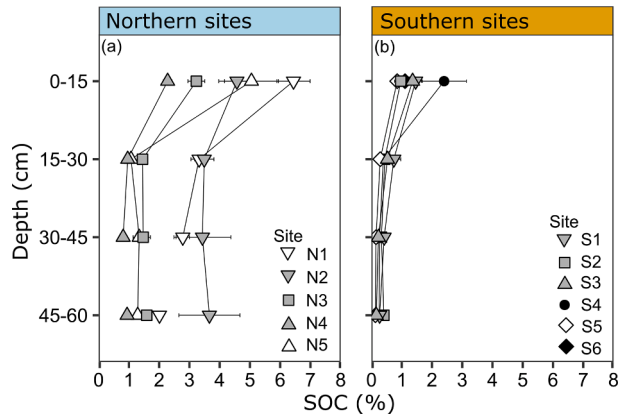

Fig. 3. Soil organic carbon content of northern (a) and southern (b) sites. The landscape gradients are indicated by grey symbols (bottom: triangle down, slope: square and top: triangle up). Additional landscape positions (S4-S6) are presented in Table 1. For site N1, N3 and N4 only one pit was sampled to 45–60 cm (see Table S1 for number of samples per depth). All other values are shown as means of all sampled pits ($n > 3$) with standard error. For an individual scaling of the SOC content see Fig. S2.

likely that these sites represent a large extent of ice-rich forest soils in the Mackenzie Delta region, which store much larger quantities of SOC in greater depth, since these ice-rich complexes can be more than 20 m thick (Ping et al., 2015; Schirrmeister et al., 2013). Deep ice-rich complexes (so called Yedoma) with average carbon contents of around 2.5% over depth and typically silty texture, are found in arctic regions of Alaska and Eurasia in former periglacial flood plains (Kanevskiy et al., 2011; Ping et al., 2015). These formations were formed during the late Pleistocene and degraded in large parts during the Holocene, which resulted in ice-rich complex remnants overlaid with younger colluvial or floodplain material (Kanevskiy et al., 2014, 2011). Due to the high SOC and ice contents, these soils are highly vulnerable to climate warming with a positive climate effect when SOC decomposition is accelerated through thaw. It is estimated that 327–466 Gt of C are stored in ice-rich complexes (e.g. Yedoma and thermokarst depositions) in Siberia, Alaska and Canada combined, which equals around 25% of the estimated total C stored in the northern circumpolar permafrost region (Strauss et al., 2017). However, the global and predominantly regional distribution of ice-rich complexes in the North Canadian permafrost region and the associated SOC stocks are largely unknown, resulting in large uncertainties of forest mineral soil SOC stocks in earth system models (Kanevskiy et al., 2011; Ping et al., 2015; Strauss et al., 2017); an urgent data gap given the spatial extent of ice-rich formations (Schuur et al., 2015).

For the southern sites under discontinuous and sporadic permafrost conditions, the total SOC stocks (0–60 cm) ranged between 26.7 and 60.2 Mg SOC ha^{-1} (Fig. 2 b). The highest total stocks were found at the downslope site (S1 = 60.2 ± 6.0 Mg SOC ha^{-1}), which were significantly higher than at the slope (S2 = 41.4 ± 3.6 Mg SOC ha^{-1}) and the sandy dune site (S5 = 26.8 ± 2.5 Mg SOC ha^{-1}). The landscape gradient showed significantly higher SOC stocks at the bottom location (S1) compared to the slope (S2), but no difference between bottom and top location (S3), indicating stable conditions at top and bottom locations in terms of soil mass transport and erosion. The SOC contents indicated a clear decrease with depth (Fig. 3 b). In the upper 0–15 cm the SOC contents ranged between 0.9 and 2.4% and were always <0.4% in 30–60 cm depth. Similarly, Shaw et al. (2018) reported SOC contents of 0.1–1.5 % on the upper 70 cm of two Regosols and two Dystric Cambisols. On average, the upper 0–15 cm contained 60 ± 3 % of the total SOC for the southern locations. The shallow lowlands soil with a fine texture (S6) contained 22.4 ± 3.7 Mg SOC ha^{-1} and so, similar amounts of SOC than the deep and sand rich Haplic Regosol (S5) in 0–60 cm (Fig. 2 b and Table 1).

3.1.2. *Implication for SOC stocks at landscape scale*

Our results suggest that SOC stocks and contents differ largely between soils under continuous and discontinuous to sporadic permafrost conditions with generally higher stocks at continuous permafrost-affected northern locations. Even within the two main regions of our study (northern and southern sites), the SOC stocks varied significantly and along two landscape gradients (of 170–580 m and 20–55 m difference in altitude, Table 1) and across landscape position. These differences were much more important in continuous permafrost and cryoturbation affected northern soils. The intensity and depth of cryoturbation depends on small-scale geomorphic changes controlling hydrological conditions and vegetation (Grosse et al., 2011; Walker et al., 2004). Hossain et al. (2007) identified in their data synthesis higher SOC stocks of mineral soils in the Boreal Plain (on average 251 Mg ha^{-1} in

0–100 cm and 154 Mg ha^{-1} in 0–50 cm), which is dominated by discontinuous and sporadic permafrost conditions, compared to the Taiga Plain (on average 195 Mg ha^{-1} in 0–100 cm and 125 Mg ha^{-1} in 0–50 cm), which is dominated by continuous permafrost conditions. This indicates an opposite trend compared to our findings. However, it needs to be taken into account that Hossain et al. (2007) only included the northern part of the Boreal Plain (South Slave Lake region) and the estimation for the Taiga Shield was based on locations predominately in the southern part of the Taiga Shield, which would only be similar to site the shallow lowland site (S6) in this study. Ultimately, our study highlights the large differences in SOC stocks across geomorphologically variable regions and challenges the generalization of SOC stocks for large ecozones (e.g. Boreal Plain with >600,000 km^2). Small-scale variations (e.g. landscape position and soil depth) need to be considered, which require more complete SOC datasets for the boreal forest soils. It also means that it is unlikely that it will be possible to predict SOC stocks from general soil properties, through, for example, pedotransfer functions and highlights the need for more local SOC measurements.

3.1.3. Importance of organic layer carbon stocks

The thickness of the organic layers varied from only 2 cm to a maximum of 35 cm, which resulted in large differences in stored C (Table 2). The C stored in the organic layers contributed to additional 12–152 Mg C ha^{-1} at northern and 11–229 Mg C ha^{-1} at southern sites, hence a large amount compared to the SOC in mineral soils (Table 2). At the northern sites, the C:N ratios ranged between 36.3 and 41.3. The C:N ratios of the southern organic layers were largest for the sand dune site (S5 = 57.5) and smallest but similar at all other sites (S1 to S4 with 29.7–31.5). The values are relatively narrow in terms of N dynamics, and are the consequence of a N-limited forest ecosystem (Högberg et al., 2017). Considering the differences in the quality of the litter and the vegetation between the sites (Table 1), the thickness of the organic layer can be assumed to be a good integrator of C stocks for a given site, and a good predictor for the composition of the total soil C stocks.

At the northern locations, similar amounts of C were located in the organic layers of the lowland sites N1 (42–152 Mg C ha^{-1}) and N2 (48–107 Mg C ha^{-1}), which had the thickest organic layers of all northern locations. The thinner organic layers at the elevated sites (N4 and N5) resulted in lower and very similar amounts of C with 12–59 Mg C ha^{-1} and 12–49 Mg C ha^{-1}, respectively. At the southern sites, the organic layer was thickest at the downslope site (S1) and contained the largest amount of C with 131–229 Mg C ha^{-1}, resulting in up to four times more C located in the organic layer than in the sampled soils of 60 cm depth. For the slope and sand dune site (S2 to S5), the additional C ranged between 11 and 66 Mg C ha^{-1} and was lowest for the shallow soil at shallow lowland site (S6) with 12–17 Mg C ha^{-1}. Thus, even thin organic layers can contain a similar or higher amount of C than the total SOC in 0–60 cm of the mineral soils at the southern locations. Consequently, organic layers are important for the C storage of boreal forest systems and need to be considered in C inventories given its high vulnerability to disturbances like wildfires (Walker et al., 2018).

Table 2
Properties of organic layers of northern (N1-N5) and southern (S1-S6) sites with the average thickness (min–max) of all sample pits (n = 9, except S6 where n = 5); the organic carbon (OC), δ^{13}C and C:N are obtained from the organic layer at the centered sampling pit (which was not determined (n.d.) for S6). The OC stocks are calculated with the average (min–max) thickness of the organic layers.

Site	Thickness (cm)	OC (g kg^{-1})	δ^{13}C (‰)	C:N (–)	OC stock[a] (Mg ha^{-1})
N1	13 (7–25)	414.7	−28.3	40.5	78 (42–152)
N2	14 (8–18)	406.7	−27.9	39.3	82 (48–107)
N3	11 (5–19)	376.2	−28.9	41.1	61 (28–105)
N4	5 (2–10)	406.1	−28.4	41.3	29 (12–59)
N5	5 (2–8)	416.2	−28.2	36.3	28 (12–49)
S1	24 (20–35)	448.3	−28.2	30.0	156 (131–229)
S2	5 (3–10)	377.2	−28.3	29.7	28 (17–55)
S3	5 (2–10)	382.5	−28.1	31.5	29 (11–56)
S4	7 (3–12)	375.6	−27.7	30.8	41 (16–66)
S5	3 (2–5)	396.8	−29.4	57.5	18 (12–29)
S6	3 (2–3)	*n.d.*			15 (12–17)[b]

[a] Estimated with an average bulk density of 0.15 g cm^{-3} obtained from a database of Canadian upland forest soils including > 2500 soil profiles presented by Shaw et al. (2018).

[b] Estimated with the average OC content of organic layers of all southern sites.

3.2. SOC quality varies with permafrost and landscape position

3.2.1. Isotopic composition and C:N ratios of SOC

The SOC in soils from the northern locations was less processed and decomposed compared to the southern locations as identified with the isotopic composition (δ^{13}C values) and C:N ratios. Compared to the mineral soil, the δ^{13}C of organic layers ranged similar to the C:N ratios only slightly between the northern and southern sites (−29.4‰ and −27.7‰; Table 2). In the soils from the northern location, the δ^{13}C of the SOC in the upper 0–15 cm ranged between −29.9‰ to −28.3‰ and remained relatively constant over depth (Fig. 4 a). The δ^{13}C values were lowest for the elevated site (N4), but varied only by 0.7‰ (−30.1 to −29.4‰) with depth. Therefore, the δ^{13}C values were similar to the isotopic composition of the organic layer over the whole profile (Table 2), especially for the lowland sites (N1 and N2). The isotopic signature of permafrost soils and ice-rich complexes has been found to be similar to the vegetation but depleted in ^{14}C, corresponding to a higher radiocarbon age (Zimov, 2006). This points to the preservation of SOC without a high degree of decomposition, which would increase the δ^{13}C values due to microbial processing (Dungait et al., 2012; Rumpel and Kögel-Knabner, 2011). We further used C:N ratios to determine plant- vs microbial-contributions to organic matter; wherein values > 14 indicate former while values < 12 indicate the latter (Kögel-Knabner, 2002). The C:N ratios were highest at the sites N1 and N5 with 27.0 ± 2.0 and 28.0 ± 1.4 in 0–15 cm, respectively (Fig. 4 c). The remaining sites showed lower and very similar values in 0–15 cm (on average 18.5 ± 0.2). In general, the C:N ratios were lower in 15–30 cm depth but remained relatively consistent in with depth for N1, N2, N3 and N5. The C:N ratios were lowest at the elevated site (N4) with increasing soil depth (7.8 ± 0.5 in 30–45 cm). In 45–60 cm depth, the C:N ratios of N1, N2 and N5 were similar with on average 16.0 ± 0.3. These high C:N ratios (>14) indicate a major contribution of plant-derived organic matter in the northern soils.

For the southern sites, the δ^{13}C values ranged between −30.2‰ and −29.0‰ in the upper 0–15 cm (Fig. 4 b). The δ^{13}C remained constant in 15–30 cm for S1 and S3, but increased at S2 to −27.3‰. The sites S1 to S4 contained inorganic carbon (pH > 6) and due to low SOC contents in greater depth (Fig. 3), the δ^{13}C could only be determined for S1, S2 and S3. The site S5, free of inorganic carbon, indicated a clear increase in δ^{13}C values with depth to −27.3 ± 0.3‰ in 45–60 cm depth. These values indicate a higher degree of SOC decomposition due to an enrichment of ^{13}C as a result of microbial processing. The C:N ratios in soils from the southern locations ranged between 14.4 and 24.1 in the upper 0–15 cm and decreased with depth for most of the sites (Fig. 4 d). The site S5 showed the highest C:N ratio in 0–15 cm (24.1 ± 2.6) and the lowest in 45–60 cm (3.6 ± 0.3), while the other sites showed values of 9.1–12.0 and thus in the range of processed SOC.

3.2.2. Mid-infrared analysis of SOC quality

The qualitative analysis of the mid-infrared spectra partially confirms the previous analyses on SOC quality using δ^{13}C values and C:N ratios. The maximum absorbance analysis of the DRIFT spectra indicated ratios of 0.7 ± 0.1 for cellulose:lignin and 1.1 ± 0.1 for aliphatic:aromatic for the organic layers of the northern locations (Fig. 5 a and b). Compared to the organic layers, the ratios in the upper 0–15 cm of the

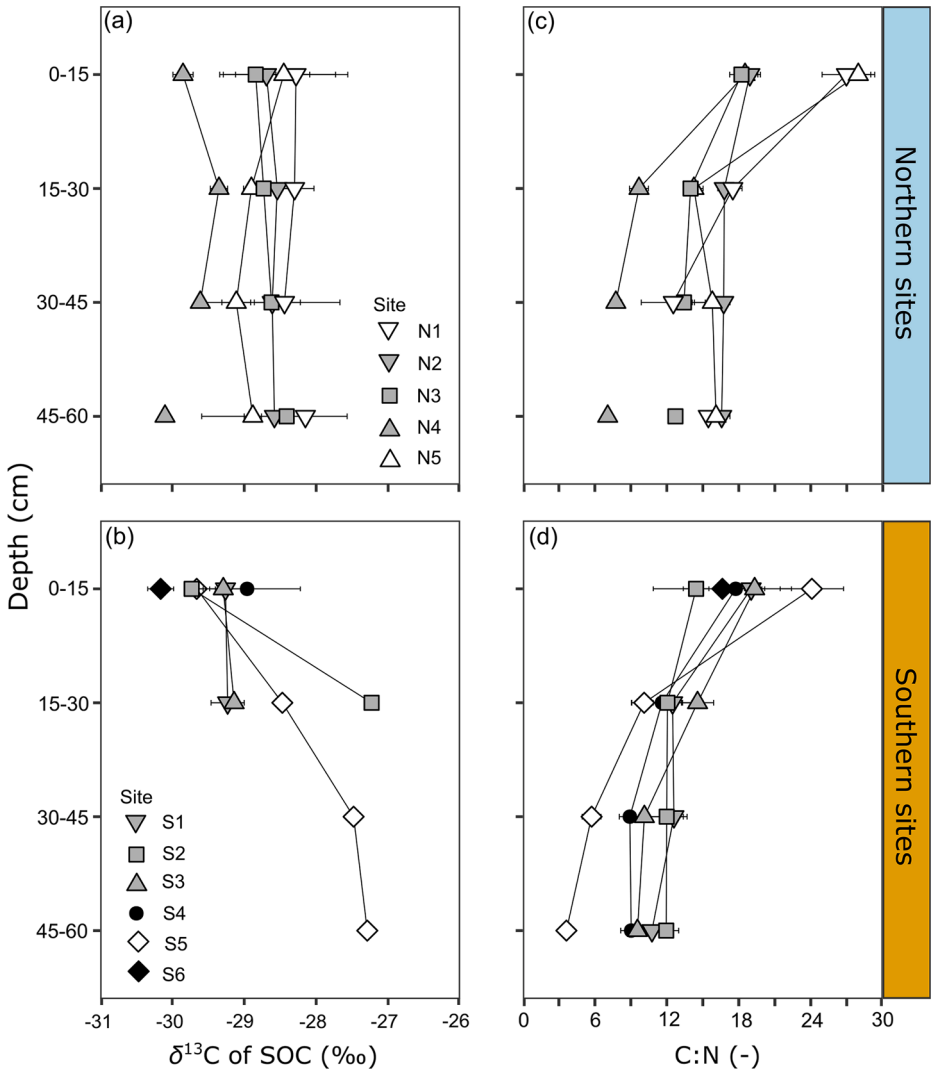

Fig. 4. δ^{13}C values and C:N ratios of SOC of northern (a and c) and southern (b and d) sites with depth. The landscape gradients are indicated by grey symbols (bottom: triangle down, slope: square and top: triangle up). Additional landscape positions (S4-S6) are presented in Table 1. For site N1, N3 and N4 only one pit was sampled to 45–60 cm (see Table S1 for number of samples per depth). All other values are shown as means of all sampled pits (n: 3–9) with standard error.

mineral soil decreased by 30 ± 6% and 26 ± 18% for the cellulose:lignin and aliphatic:aromatic ratios, respectively. The cellulose:lignin ratios were 12 to 24% higher in the upper 0–15 cm compared to the organic layer at the elevated sites N4 and N5, while they were 40 to 65% lower in the soils of the lowland and at the slope (N1-N3). The sites N4 and N5 indicated high proportions of cellulose in depths below 15 cm with ratios of 2.2–7.1. This semi-quantitative but SOC compound-specific analysis suggested that northern sites have SOC with a large proportion of minimally processed organic matter remaining in a similar state and relative composition as the organic layer.

For the southern sites, the organic layers showed cellulose:lignin ratios of 0.8 ± 0.1 and aliphatic:aromatic ratios of 0.6 ± 0.1 (Fig. 5 c and d). In the upper 0–15 cm of mineral soil, these ratios decreased by on average 55 ± 4% and 82 ± 2% for cellulose:lignin and aliphatic:aromatic, respectively. Most of the soils indicated further decreases in the ratios and thus an increasing proportion of lignin- and aromatic-derived compounds. This supports the previous findings (narrowing C:N ratios and increased δ^{13}C values) of a higher proportion of processed SOC in the southern soils under discontinuous and sporadic permafrost conditions, relative to the northern sites. The degradation resulted in an enrichment of aromatic and lignin-like compounds as compared to the organic layer, which is more enriched in aliphatic- and cellulose-like compounds (Rumpel and Kögel-Knabner, 2011) and indicated higher ratios (Fig. 5 b and d).

The northern soil DRIFT spectra indicated higher contents of aliphatic compounds with 50% higher aliphatic:aromatic ratios compared to the southern soils over the whole mineral soil profiles. This difference is smaller for the organic layers (17% higher ratios at northern sites). Similarly, the cellulose:lignin ratios were 91% higher (73% when excluding N4 and N5) over all soil depths, which was also a larger difference than between the organic layers (24% higher ratios at northern sites). These findings can be influenced by differences in the vegetation (spruce or pine dominated stands, Table 1) and thus a different composition of the initial organic matter entering the soil system. However, due the direct comparison of δ^{13}C values, C:N ratios and DRIFT spectra to the composition of the organic layers, it is most likely that large parts of the SOC in cryoturbated soils from the northern locations are not processed and thus vulnerable for decomposition with warming and environmental change (Ping et al., 2015; Tarnocai et al., 2009). Warming-related permafrost thaw is expected to increase microbial activity in mineral permafrost soils and subsequently increase the C emissions (Chen et al., 2021; Schädel et al., 2016), especially in soils with a large proportion of minimally processed or labile SOC with a potential of fast cycling may cause rapid positive feedback due to aerobic and anaerobic decomposition (Knoblauch et al., 2013; Schuur et al., 2015).

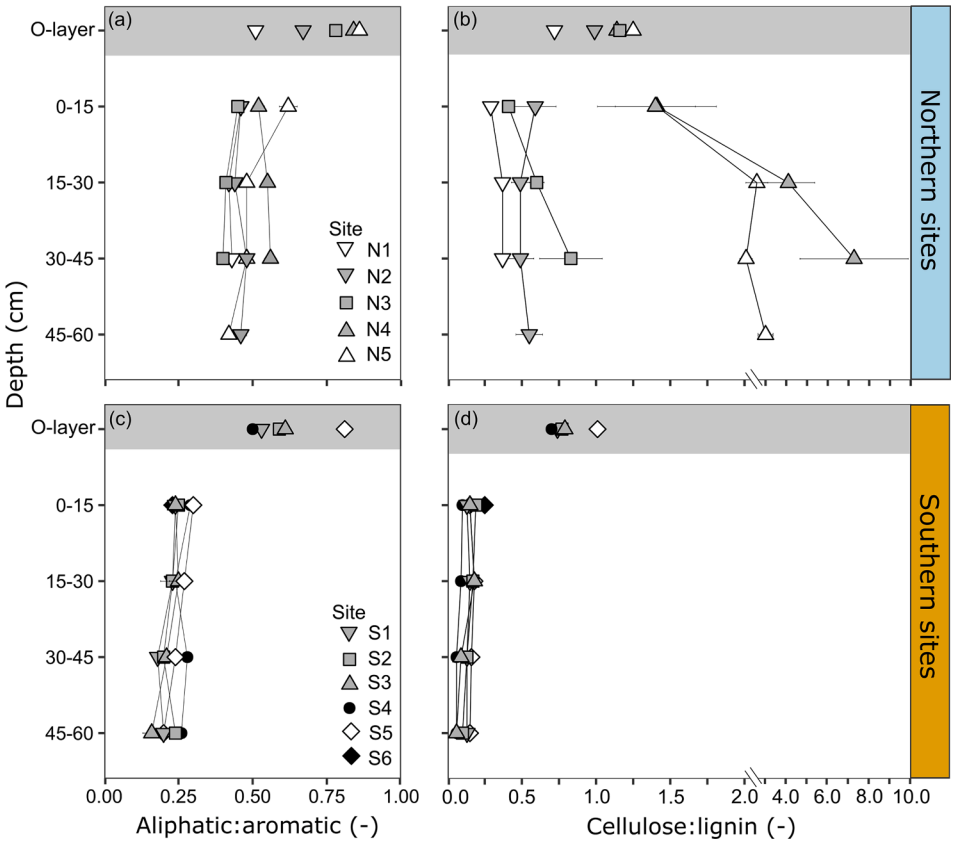

Fig. 5. Ratio of maximum absorption of cellulose (band 1245 cm^{-1}) to lignin (band 1508 cm^{-1}) and aliphatic (band 2930 cm^{-1}) to aromatic (band 1630 cm^{-1}) compounds obtained with DRIFT analysis for the organic layers and all sampled soil depths for northern (a and b) and southern (c and d) sites. The landscape gradients are indicated by grey symbols (bottom: triangle down, slope: square and top: triangle up). Additional landscape positions (S4-S6) are presented in Table 1. All values are shown as means of all sampled pits (n: 3–9) with standard error (in most cases the error is smaller than the symbol). Note the change in the x-axes for cellulose:lignin ratios (b and d) and see Fig. S3 for details.

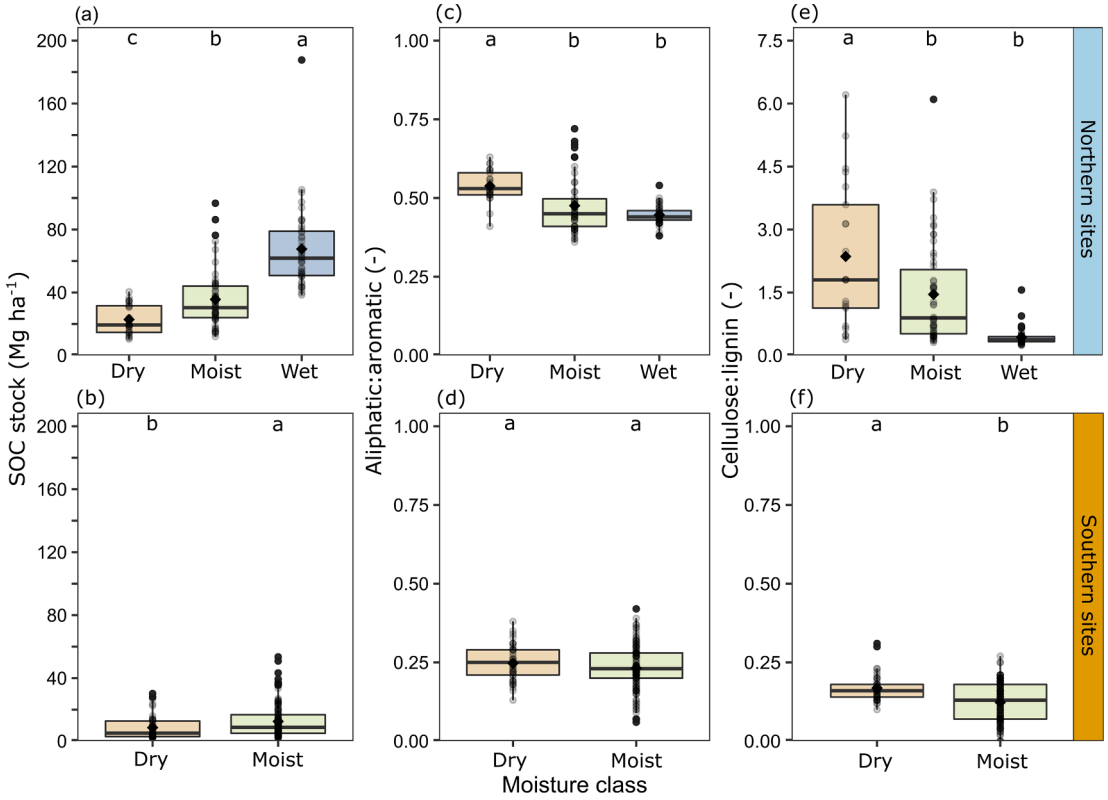

Fig. 6. SOC stocks, ratio of aliphatic:aromatic and cellulose:lignin with moisture classes of northern (a, c and e) and southern (b, d and f) sites. The data was aggregated over all depth for each moisture class. The mean value is shown as a diamond and letters indicate significant differences between moisture classes ($p < 0.05$). Note the differences in y-axes scaling for the cellulose:lignin ratios (e and f).

3.3. Site moisture as controlling factor of SOC stocks and quality

Site moisture was the dominant factor controlling SOC stocks at both northern and southern sites with significantly higher stocks with increasing moisture (Fig. 6 a and b). The higher SOC stocks at moist and wet sites can be explained with a general higher input of organic matter due to a higher net primary production of the vegetation, resulting also in a faster accumulation of organic matter and thicker organic layers (Table 2). In general, it is assumed that moist conditions promote the conservation of SOC in boreal soils and well-drained soil conditions favor the decomposition, which holds true for organic soils (Fenner and Freeman, 2011). The heterotrophic soil respiration and thus the microbial activity is highly dependent on soil moisture, especially for mineral soils, with a reduced respiration under dry conditions (Moyano et al., 2012).

The SOC quality, determined through the cellulose:lignin and aliphatic:aromatic ratios, also varied with site moisture. At the northern sites, the aliphatic:aromatic and cellulose:lignin ratios were similar at moist and wet sites, but significantly lower ($p < 0.05$) than dry sites (Fig. 6 c and e). This indicates a higher proportion of aromatic- and lignin-like compounds with increasing site moisture and thus a potentially higher degree of SOC decomposition than at dryer sites. This difference in SOC quality may have two origins. On the one hand, the vegetation differs, and so the SOC quality, since the ratios of cellulose: lignin and aliphatic:aromatic vary also between the organic layers with higher ratios (more input of cellulose and aliphatic like compounds) at the dry sites compared to the moist and wet sites (Fig. 5 and Table 1). On the other hand, the dry conditions, especially of the elevated northern sites (N4 and N5) with high exposure to wind and snow, may have reduced the decomposition rate of SOC, while the cycling is faster in the lowland and more moist soils (N1 and N2). For the southern sites, a significant higher proportion of lignin, as indicated by smaller cellulose: lignin ratios, was observed with increasing site moisture ($p < 0.05$, Fig. 6 f). However, the aliphatic:aromatic ratios indicated no significant trend (Fig. 6 d). This indicates that the SOC of the southern soils may be more controlled by the vegetation and the initial composition of the input organic matter controlling the composition of already microbial processed SOC, compared to the northern soils.

Soil properties showed a weak relationship with SOC contents of soils from the northern and southern sites. In soils from the north, only the CEC_{eff} (linear regression $R^2 = 0.52$; $p < 0.05$) indicated a weak positive relationship with the SOC contents, but not for other soil properties (pH_{CaCl2}, clay and silt content, total Fe and Al; Fig. S4). For the southern sites, the SOC contents showed a weak but positive relationship with the CEC_{eff} (linear regression $R^2 = 0.52$; $p < 0.05$) and silt content (linear regression $R^2 = 0.26$; $p < 0.05$) and no relationship with the other soil properties (Fig. S5). The CEC_{eff} can directly be controlled by the SOC (Solly et al., 2020), which may explain the observed relationship in the SOC-rich soils from the northern sites, while in contrast, the texture and elemental composition may be of little importance in mineral soils under continuous permafrost conditions. The relationship of SOC with silt and CEC_{eff} in the southern soils indicates that a relatively fine soil texture (in these soils potentially controlled by silt due to low weathering, which results in low clay contents; Table 1 and S1) may promote higher SOC contents and thus the soil texture maybe more important in soils under discontinuous permafrost conditions with a higher degree of SOC decomposition.

All observed relationships with soil properties were weak and less pronounced compared to the relationship with site moisture, which suggests that the site-specific moisture conditions, landscape position and associated vegetation are more important for SOC dynamics in permafrost-affected soils, which is in agreement with Grosse et al. (2011). It needs to be noticed that the northern and southern sites differ not only largely in SOC dynamics and soil properties (Table. 1), but also in the landscape history with around 2 ka difference in deglaciation and soil forming parent materials (section 2.1). While we aimed to studying SOC dynamics in forest mineral soils under two main permafrost conditions (continuous and discontinuous to sporadic), complete gradients covering a variety of parent material and along latitudes would be needed to identify the effect of soil parameters and also pedogenesis on SOC dynamics and quality.

The moisture classification used in this study is based on the topographic drainage, permafrost status and soil texture (Johnstone et al., 2008). Therefore, similar to SOC stocks, SOC quality of mineral soils in high latitude areas is driven by small-scale geomorphic differences controlling drainage and permafrost conditions. These small-scale differences are important to consider when evaluating the response of boreal forest soils to global change and warming (Schuur et al., 2015; Turetsky et al., 2020).

3.4. SOC stock prediction with mid-infrared spectra

The chemometric prediction of SOC using DRIFT spectra and PLSR showed good agreement with the measured SOC contents at both the northern and southern sites. The prediction was better for the continuously permafrost-affected northern soils ($R^2 = 0.94$ and RMSE of 0.41% SOC) compared to the southern soils (R^2: 0.83 and RMSE of 0.29% SOC; Fig. S8). It was also possible to predict a similar depth distribution and thus similar dynamics compared to the measured SOC contents in the soil profiles of all sites (Fig. S9). Matamala et al. (2019) incubated tundra soils at different temperatures (1–16 °C) in order to predict total and decomposable SOC. The authors reported a very high precision of SOC content prediction using PLSR and DRIFT spectra for the permafrost-affected soils in their study using four sites and three depths ($R^2 = 0.99$ and RMSE = 0.01% SOC). Using > 50,000 spectra from the National Cooperative Soil Survey Soil Characterization Data, Sanderman et al. (2020) predicted SOC contents and several soil parameters with high precision ($R^2 > 0.80$) of soils across the United States. The authors reported a good prediction of SOC with soil depth along the profiles ($R^2 = 0.99$) and a RMSE of 0.64% SOC. Helfenstein et al. (2021) predicted SOC contents of temperate peatland soils in Switzerland with up to 52% of total C with and RMSEs of 2–3% SOC ($R^2 > 0.9$) and consistently lower RMSE (<1%) for soils with a maximum of 10% SOC in combination of local datasets and the Swiss soil spatial libraries (SSL). Nocita et al. (2014) used > 19,000 DRIFT spectra from soils (0–20 cm) of the European Land Use/Cover Area frame Statistical Survey (LUCAS) and predicted SOC contents with high precision in crop- and grassland (RMSE of 0.36–0.72% SOC), but with less precision for forest (RMSE of 1.19% SOC) and organic soils (RMSE of 5.11% SOC). Thus, our prediction of SOC contents in boreal forest soils is in the same magnitude range of SOC prediction performance in soils across different climatic zones with a broad range of low and high SOC contents.

Given the sufficient prediction of SOC contents, the SOC stocks were also well predicted for the northern ($R^2 = 0.85$ and RMSE = 0.10 log(Mg ha^{-1})) and southern sites ($R^2 = 0.82$ and RMSE = 0.15 log(Mg ha^{-1}); Fig. 7 a and b). While, RMSE and R^2 are good statistical parameters to evaluate the general model performance, but they may not be useful to evaluate the actual uncertainty of prediction (Dangal et al., 2019). We evaluated the uncertainty of the predicted SOC stocks in our soils as a function of the measured SOC stocks. The absolute deviation of measured and predicted SOC stocks increased with increasing SOC stocks (Fig. S10 and S11). However, the relative deviation of measured and predicted SOC stocks, including over- and underpredictions, was on average 14% for the soils from northern sites and 23% for the soils form the southern sites. The uncertainty ranged from a maximal underestimation of 42% and 60% and a maximal overestimation of 54% and 129% for northern and southern sites, respectively. However, 75% (northern sites) and 64% (southern sites) of all predicted values were within a 20% difference from measured SOC stocks (Fig. S10 and S11). In comparison, the average coefficient of variation of the measured SOC stocks (CV) over all sampling depths, as an indicator for the spatial variation within the 30x30 m sampling plots, represented 29 ± 12% for

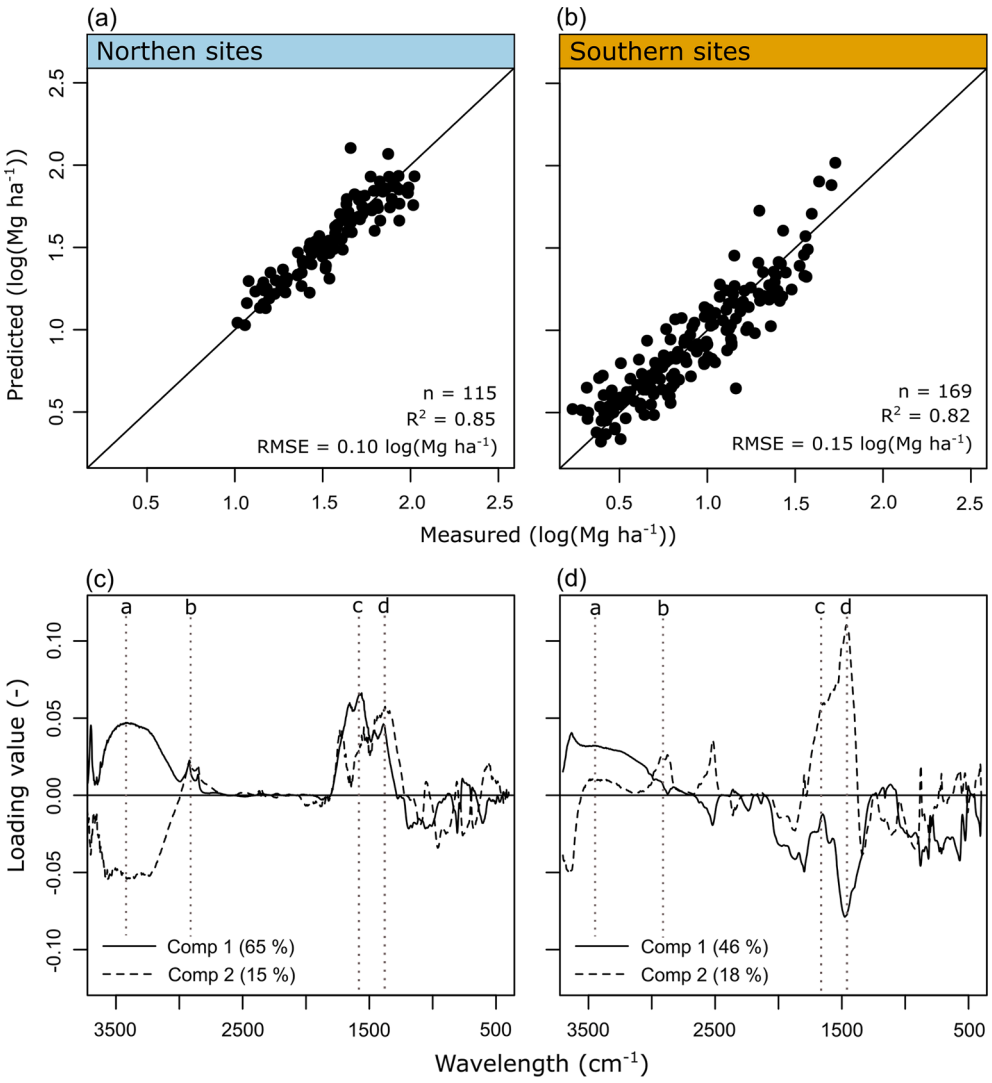

Fig. 7. Measured and predicted SOC stocks [log(Mg ha^{-1})] and prediction contribution of spectra regions (loading values) for the first two components (with percentage of explained variance) for northern (a and c) and southern (b and d) sites. With bands a = 3600–3100 cm^{-1}, phenolic, alcoholic and carboxylic (—OH) compounds; b = 2940–2920 cm^{-1}, aliphatic (C—H) compounds; c = 1660–1590 cm^{-1}, aromatic (C═C) compounds and d = 1500–1420 cm^{-1}, aromatic and lignin like (C═C) compounds.

soils from the northern and 41 ± 16% for the soils form the southern sites. Compared to these values, the prediction of SOC stocks using DRIFT in combination with PLSR was in a similar or lower range as the spatial heterogeneity of SOC stocks obtained from field measurements in this study.

The SOC stock prediction highlights the differences in SOC composition between the northern and southern sites. The importance of the different mid-infrared wavelengths considered for the prediction is indicated as the loading values of the PLSR (Fig. 7 c and d). The loadings of the SOC content prediction were similar to the SOC stocks predictions (Fig. S8). To predict the SOC stocks in the northern soils, the absorption of bands assigned to aliphatic (regions a and b in Fig. 7) and aromatic compounds (regions c and d in Fig. 7) were most important to predict the main variability (65% with the first component). For the southern sites, these wavelengths contributed negatively to the prediction; but nearly half of the variance was explained with bands at 1450–1600 cm^{-1} (regions c and d in Fig. 7). This negative contribution to the prediction, assigned to aromatic compounds, could mean that low aromatic functions correspond to high SOC in the first explanation of variances (first component). Nevertheless, the mineral phase of a soil is also represented in mid-infrared spectra and the mentioned regions can be interfered by mainly clay minerals (Reeves, 2012) or the spectra can be shifted due to interactions of cations with the organic matter (Ellerbrock and Gerke, 2021). This may constitute a limitation of SOC prediction in soils with a higher degree of SOC decomposition.

The good prediction of SOC in permafrost soils was previously discussed and assigned to the preservation of compounds and functional groups, which allow a well-defined DRIFT spectra (Calderón et al., 2017; Matamala et al., 2019, 2017; Tinti et al., 2015). The better prediction of SOC stocks in the northern soils compared to the southern soils in our study suggests that the high SOC contents with a limited degree of degradation, as discussed previously (Figs. 4 and 5), are relatively easy to predict using DRIFT spectra, which offers a promising alternative for these undersampled soils of remote northern regions.

3.5. Potential of SOC stock predictions

The limited number of observations from high-latitude soils contribute to large uncertainties in global SOC estimations and earth system model simulations (Hugelius et al., 2014). Uncertainties originating from permafrost thaw feedbacks, for example, which explain half of the total uncertainty of climate models using the high emission representative concentration pathway (RCP 8.5 as in Burke et al. (2012)). Not only the limited number but also lack of comprehensive SOC observations and spatial distribution, and mainly SOC stock data, causes these uncertainties (Dai et al., 2019; Luo et al., 2016; Poggio et al., 2021). Data on SOC stocks above 60° north is scarce for the Canadian boreal soils (Fig. S12 for data in our study region, Shaw et al. (2018)). Additionally, uncertainties of SOC estimations in high-latitude soils can be associated to the vertical heterogeneity of SOC contents in

soils affected by cryoturbation (Shu et al., 2020). Our study suggested that a combination of mid-infrared and PLSR is suitable to predict SOC of Canadian boreal forest mineral soils across the landscape and soil depth, which offers a promising alternative to fill data gaps and reduce uncertainties originated from high latitude regions. We further elucidate that SOC stock and content predictions can vary in terms of precision and the explanatory wavelengths used between different regions (e.g. continuous vs. discontinuous permafrost) and recommend that local limitations should be considered in future studies.

4. Conclusion

Our study quantified the magnitude, variability and drivers of SOC stocks and quality for under-studied high-latitude mineral soils. We found that SOC stocks in boreal forest mineral soils of northern Canada can be four times higher under continuous permafrost conditions compared to soils under discontinuous or sporadic permafrost. The organic layer was identified as a significant C pool of boreal forest soils and can contain similar amounts or more C than the upper 60 cm of the mineral soils under discontinuous permafrost, even if the organic layers are thin (2–35 cm). The SOC stocks varied largely with small-scale geomorphic changes (along gradients of < 580 m) and were significantly higher with increasing site moisture in flat lowland areas. Site moisture controlled the quality and cycling of SOC, which may indicate a general higher input of organic matter at moist sites, but also a faster cycling compared to elevated dryer sites. Cryoturbated soils showed large amounts of C at depth with up to 70% of total SOC in > 15 cm depth, while around 60% of the total SOC of soils under discontinuous permafrost was located in the upper 15 cm. Furthermore, soils under continuous permafrost showed a higher proportion of minimally decomposed organic matter compared to soils under discontinuous to sporadic permafrost as indicated by the isotopic composition similar to the organic layers and higher proportion of aliphatic- and cellulose-like compounds. This suggests that boreal forest mineral soils can contain a large decomposable SOC fraction, which may quickly respond to climate change. Mid-infrared spectra and PLSR analyses were well-suited to SOC stock prediction for our sites. The prediction was better in soils containing less microbially processed SOC as found under continuous permafrost conditions. However, the prediction was sensitive to SOC distribution in the soil profiles and had smaller uncertainties (14–23% prediction error) than the observed spatial variability of SOC stocks in continuous and discontinuous permafrost soils. We showed that chemometric approaches offer a promising tool to fill data gaps of SOC stocks from high-latitude mineral soils and minimize global uncertainties of SOC stocks.

Declaration of Competing Interest

The authors declare that they have no known competing financial interests or personal relationships that could have appeared to influence the work reported in this paper.

Acknowledgements

The authors gratefully acknowledge the Community of the Northwest Territory Métis Nation (Fort Smith) and the Aurora Research Institute for logistical and security support during fieldwork. The authors acknowledge the Wood Buffalo National Park for support during site selection and permitting access to the park for the fieldwork.

Funding

This work was funded by the Swiss National Science Foundation (grant no. 200021_178768).

Author contribution

SA acquired the funding. MS and SA conceptualized the fieldwork. MS and SLB designed and conducted the fieldwork. MS conducted the laboratory work and data preparation. MS, SA and AM analyzed the data. MS wrote the manuscript with contribution of all co-authors. All authors approved the final manuscript.

Data availability

The data related to this article are available upon request from the corresponding author and available online on Zenodo (10.5281/zenodo.6024831).

Appendix A. Supplementary material

Supplementary data to this article can be found online at https://doi.org/10.1016/j.catena.2022.106194.

References

Agriculture and Agri-Food Canada, 2013. National ecological framework for Canada. Government of Canada; Agriculture and Agri-Food Canada. URL: https://open.canada.ca/data/en/dataset/3ef8e8a9-8d05-4fea-a8bf-7f5023d2b6e1 (accessed February 2022).

Batjes, N.H., Ribeiro, E., van Oostrum, A.d., 2019. Standardised soil profile data to support global mapping and modelling (WoSIS snapshot 2019). Earth Syst. Sci. Data 12 (1), 299–320. https://doi.org/10.5194/essd-12-299-2020.

Bellon-Maurel, V., McBratney, A., 2011. Near-infrared (NIR) and mid-infrared (MIR) spectroscopic techniques for assessing the amount of carbon stock in soils – Critical review and research perspectives. Soil Biol. Biochem. 43 (7), 1398–1410. https://doi.org/10.1016/j.soilbio.2011.02.019.

Biskaborn, B.K., Smith, S.L., Noetzli, J., Matthes, H., Vieira, G., Streletskiy, D.A., Schoeneich, P., Romanovsky, V.E., Lewkowicz, A.G., Abramov, A., Allard, M., Boike, J., Cable, W.L., Christiansen, H.H., Delaloye, R., Diekmann, B., Drozdov, D., Etzelmüller, B., Grosse, G., Guglielmin, M., Ingeman-Nielsen, T., Isaksen, K., Ishikawa, M., Johansson, M., Johannsson, H., Joo, A., Kaverin, D., Kholodov, A., Konstantinov, P., Kröger, T., Lambiel, C., Lanckman, J.-P., Luo, D., Malkova, G., Meiklejohn, I., Moskalenko, N., Oliva, M., Phillips, M., Ramos, M., Sannel, A.B.K., Sergeev, D., Seybold, C., Skryabin, P., Vasiliev, A., Wu, Q., Yoshikawa, K., Zheleznyak, M., Lantuit, H., 2019. Permafrost is warming at a global scale. Nat. Commun. 10, 264. https://doi.org/10.1038/s41467-018-08240-4.

Bisutti, I., Hilke, I., Raessler, M., 2004. Determination of total organic carbon – an overview of current methods. Trends Anal. Chem. 23 (10-11), 716–726. https://doi.org/10.1016/j.trac.2004.09.003.

Bockheim, J.G., 2007. Importance of cryoturbation in redistributing organic carbon in permafrost-affected soils. Soil Sci. Soc. Am. J. 71 (4), 1335–1342. https://doi.org/10.2136/sssaj2006.0414N.

Brandt, J.P., Flannigan, M.D., Maynard, D.G., Thompson, I.D., Volney, W.J.A., 2013. An introduction to Canada's boreal zone: ecosystem processes, health, sustainability, and environmental issues. Environ. Rev. 21 (4), 207–226. https://doi.org/10.1139/er-2013-0040.

Burke, E.J., Hartley, I.P., Jones, C.D., 2012. Uncertainties in the global temperature change caused by carbon release from permafrost thawing. Cryosphere 6, 1063–1076. https://doi.org/10.5194/tc-6-1063-2012.

Calderón, F.J., Culman, S., Six, J., Franzluebbers, A.J., Schipanski, M., Beniston, J., Grandy, S., Kong, A.Y.Y., 2017. Quantification of soil permanganate oxidizable C (POXC) using infrared spectroscopy. Soil Sci. Soc. Am. J. 81 (2), 277–288. https://doi.org/10.2136/sssaj2016.07.0216.

Camill, P., 2005. Permafrost thaw accelerates in boreal peatlands during late-20th century climate warming. Clim. Change 68 (1-2), 135–152. https://doi.org/10.1007/s10584-005-4785-y.

Carter, M.R., Gregorich, E.G. (Eds.), 2008. Soil sampling and methods of analysis, 2nd ed. Canadian Society of Soil Science, CRC Press, Boca Raton, FL.

Chadburn, S.E., Burke, E.J., Cox, P.M., Friedlingstein, P., Hugelius, G., Westermann, S., 2017. An observation-based constraint on permafrost loss as a function of global warming. Nat. Clim. Change 7 (5), 340–344. https://doi.org/10.1038/nclimate3262.

Chen, Y., Liu, F., Kang, L., Zhang, D., Kou, D., Mao, C., Qin, S., Zhang, Q., Yang, Y., 2021. Large-scale evidence for microbial response and associated carbon release after permafrost thaw. Glob. Change Biol. 27 (14), 3218–3229. https://doi.org/10.1111/gcb.15487.

Cotrufo, M.F., Boot, C., Abiven, S., Foster, E.J., Haddix, M., Reisser, M., Wurster, C.M., Bird, M.I., Schmidt, M.W.I., 2016. Quantification of pyrogenic carbon in the environment: An integration of analytical approaches. Org Geochem. 100, 42–50. https://doi.org/10.1016/j.orggeochem.2016.07.007.

Dai, Y., Shangguan, W., Wei, N., Xin, Q., Yuan, H., Zhang, S., Liu, S., Lu, X., Wang, D., Yan, F., 2019. A review of the global soil property maps for earth system models. SOIL 5, 137–158. https://doi.org/10.5194/soil-5-137-2019.

Dalton, A.S., Margold, M., Stokes, C.R., Tarasov, L., Dyke, A.S., Adams, R.S., Allard, S., Arends, H.E., Atkinson, N., Attig, J.W., Barnett, P.J., Barnett, R.L., Batterson, M., Bernatchez, P., Borns, H.W., Breckenridge, A., Briner, J.P., Brouard, E., Campbell, J. E., Carlson, A.E., Clague, J.J., Curry, B.B., Daigneault, R.-A., Dubé-Loubert, H., Easterbrook, D.J., Franzi, D.A., Friedrich, H.G., Funder, S., Gauthier, M.S., Gowan, A.S., Harris, K.L., Hétu, B., Hooyer, T.S., Jennings, C.E., Johnson, M.D., Kehew, A.E., Kelley, S.E., Kerr, D., King, E.L., Kjeldsen, K.K., Knaeble, A.R., Lajeunesse, P., Lakeman, T.R., Lamothe, M., Larson, P., Lavoie, M., Loope, H.M., Lowell, T.V., Lusardi, B.A., Manz, L., McMartin, I., Nixon, F.C., Occhietti, S., Parkhill, M.A., Piper, D.J.W., Pronk, A.G., Richard, P.J.H., Ridge, J.C., Ross, M., Roy, M., Seaman, A., Shaw, J., Stea, R.R., Teller, J.T., Thompson, W.B., Thorleifson, L.H., Utting, D.J., Veillette, J.J., Ward, B.C., Weddle, T.K., Wright, H.E., 2020. An updated radiocarbon-based ice margin chronology for the last deglaciation of the North American ice sheet complex. Quat. Sci. Rev. 234, 106223. https://doi.org/10.1016/j.quascirev.2020.106223.

Dangal, S., Sanderman, J., Wills, S., Ramirez-Lopez, L., 2019. Accurate and precise prediction of soil properties from a large mid-infrared spectral library. Soil Syst. 3, 11. https://doi.org/10.3390/soilsystems3010011.

Dungait, J.A.J., Hopkins, D.W., Gregory, A.S., Whitmore, A.P., 2012. Soil organic matter turnover is governed by accessibility not recalcitrance. Glob. Change Biol. 18 (6), 1781–1796. https://doi.org/10.1111/j.1365-2486.2012.02665.x.

Ecosystem Classification Group, 2007. Ecological regions of the Northwest Territories – Taiga Plains. Department of Environment and Natural Resources, Government of the Northwest Territories, Yellowknife, NT, Canada.

Ellerbrock, R.H., Gerke, H.H., 2021. FTIR spectral band shifts explained by OM–cation interactions. J. Plant Nutr. Soil Sci. 184 (3), 388–397. https://doi.org/10.1002/jpln.202100056.

Erdozain, M., Freeman, E.C., Ouellet Dallaire, C., Teichert, S., Nelson, H.W., Creed, I.F., 2019. Demand for provisioning ecosystem services as a driver of change in the Canadian boreal zone. Environ. Rev. 27, 166–184. https://doi.org/10.1139/er-2018-0064.

FAO, 2014. World reference base for soil resources 2014. International soil classification system for naming soils and creating legends for soil maps, World Soil Resources Reports No. 106. Food and Agriculture Organisation of the United Nations, Rome.

Fenner, N., Freeman, C., 2011. Drought-induced carbon loss in peatlands. Nat. Geosci. 4 (12), 895–900. https://doi.org/10.1038/ngeo1323.

Grosse, G., Harden, J., Turetsky, M., McGuire, A.D., Camill, P., Tarnocai, C., Frolking, S., Schuur, E.A.G., Jorgenson, T., Marchenko, S., Romanovsky, V., Wickland, K.P., French, N., Waldrop, M., Bourgeau-Chavez, L., Striegl, R.G., 2011. Vulnerability of high-latitude soil organic carbon in North America to disturbance. J. Geophys. Res. Biogeosci. 116, 1–23. https://doi.org/10.1029/2010JG001507.

Gruber, S., 2012. Derivation and analysis of a high-resolution estimate of global permafrost zonation. Cryosphere 6, 221–233. https://doi.org/10.5194/tc-6-221-2012.

Helbig, M., Pappas, C., Sonnentag, O., 2016. Permafrost thaw and wildfire: Equally important drivers of boreal tree cover changes in the Taiga Plains, Canada. Geophys. Res. Lett. 43 (4), 1598–1606. https://doi.org/10.1002/2015GL067193.

Helfenstein, A., Baumann, P., Viscarra Rossel, R., Gubler, A., Oechslin, S., Six, J., 2021. Quantifying soil carbon in temperate peatlands using a mid-IR soil spectral library. SOIL 7, 193–215. https://doi.org/10.5194/soil-7-193-2021.

Högberg, P., Näsholm, T., Franklin, O., Högberg, M.N., 2017. Tamm Review: On the nature of the nitrogen limitation to plant growth in Fennoscandian boreal forests. For. Ecol. Manage. 403, 161–185. https://doi.org/10.1016/j.foreco.2017.04.045.

Hossain, M.F., Zhang, Y.u., Chen, W., Wang, J., Pavlic, G., 2007. Soil organic carbon content in northern Canada: A database of field measurements and its analysis. Can. J. Soil Sci. 87 (3), 259–268. https://doi.org/10.4141/S06-029.

Hothorn, T., Bretz, F., Westerfall, P., Heoberger, R.M., Schuetzenmeister, A., Scheibe, S., 2021. Multcomp package: Simultaneous inference in general parametric models (Version1.4-17). els (Version1.4-17). URL: http://multcomp.R-forge.R-project.org (accessed February 2022).

Hugelius, G., Loisel, J., Chadburn, S., Jackson, R.B., Jones, M., MacDonald, G., Marushchak, M., Olefeldt, D., Packalen, M., Siewert, M.B., Treat, C., Turetsky, M., Voigt, C., Yu, Z., 2020. Large stocks of peatland carbon and nitrogen are vulnerable to permafrost thaw. PNAS 117 (34), 20438–20446. https://doi.org/10.1073/pnas.1916387117.

Hugelius, G., Strauss, J., Zubrzycki, S., Harden, J.W., Schuur, E.A.G., Ping, C.-L., Schirrmeister, L., Grosse, G., Michaelson, G.J., Koven, C.D., O'Donnell, J.A., Elberling, B., Mishra, U., Camill, P., Yu, Z., Palmtag, J., Kuhry, P., 2014. Estimated stocks of circumpolar permafrost carbon with quantified uncertainty ranges and identified data gaps. Biogeosciences 11 (23), 6573–6593. https://doi.org/10.5194/bg-11-6573-2014.

IPCC, 2013. Climate change 2013: The physical science basis. Contribution of working group I to the fifth assessment report of the Intergovernmental Panel on Climate Change. Stocker, T.F., Qin, D., Plattner, G.-K., Tignor, M., Allen, S.K., Boschung, J., Nauels, A., Xia, Y., Bex, V., Midgley, P.M. (Eds.), Cambridge University Press, Cambridge, United Kingdom and New York, NY, USA, p. 1535.

Jackson, R.B., Lajtha, K., Crow, S.E., Hugelius, G., Kramer, M.G., Piñeiro, G., 2017. The ecology of soil carbon: Pools, vulnerabilities, and biotic and abiotic controls. Annu. Rev. Ecol. Evol. Syst. 48 (1), 419–445. https://doi.org/10.1146/annurev-ecolsys-112414-054234.

Jobbágy, E.G., Jackson, R.B., 2000. The vertical distribution of soil organic carbon and its relation to climate and vegetation. Belowground Process. Global Change 10 (2), 423–436. https://doi.org/10.2307/2641104.

Johnstone, J.F., Hollingsworth, T.N., Chapin III, F.S., 2008. A key for predicting postfire successional trajectories in black spruce stands of interior Alaska. U.S. Department of Agriculture, Forest Service, Pacific Northwest Research Station, Portland, OR.

Kaiser, C., Meyer, H., Biasi, C., Rusalimova, O., Barsukov, P., Richter, A., 2007. Conservation of soil organic matter through cryoturbation in arctic soils in Siberia. J. Geophys. Res. 112, G02017. https://doi.org/10.1029/2006JG000258.

Kanevskiy, M., Jorgenson, T., Shur, Y., O'Donnell, J.A., Harden, J.W., Zhuang, Q., Fortier, D., 2014. Cryostratigraphy and permafrost evolution in the lacustrine lowlands of west-central Alaska. Permafrost Periglac. Process 25 (1), 14–34. https://doi.org/10.1002/ppp.1800.

Kanevskiy, M., Shur, Y., Fortier, D., Jorgenson, M.T., Stephani, E., 2011. Cryostratigraphy of late pleistocene syngenetic permafrost (yedoma) in northern Alaska, Itkillik River exposure. Quat. Res. 75 (3), 584–596. https://doi.org/10.1016/j.yqres.2010.12.003.

Knoblauch, C., Beer, C., Sosnin, A., Wagner, D., Pfeiffer, E.-M., 2013. Predicting long-term carbon mineralization and trace gas production from thawing permafrost of Northeast Siberia. Glob. Change Biol. 19 (4), 1160–1172. https://doi.org/10.1111/gcb.12116.

Köchy, M., Hiederer, R., Freibauer, A., 2015. Global distribution of soil organic carbon – Part 1: Masses and frequency distributions of SOC stocks for the tropics, permafrost regions, wetlands, and the world. Soil 1 (1), 351–365. https://doi.org/10.5194/soil-1-351-201510.5194/soil-1-351-2015-supplement.

Kögel-Knabner, I., 2002. The macromolecular organic composition of plant and microbial residues as inputs to soil organic matter. Soil Biol. Biochem. 34, 139–162. https://doi.org/10.1016/j.soilbio.2016.08.011.

Kurz, W.A., Shaw, C.H., Boisvenue, C., Stinson, G., Metsaranta, J., Leckie, D., Dyk, A., Smyth, C., Neilson, E.T., 2013. Carbon in Canada's boreal forest — A synthesis. Environ. Rev. 21 (4), 260–292. https://doi.org/10.1139/er-2013-0041.

Kvalheim, O.M., Arneberg, R., Grung, B., Rajalahti, T., 2018. Determination of optimum number of components in partial least squares regression from distributions of the root-mean-squared error obtained by Monte Carlo resampling: Determination of optimum number of components in PLS regression. J. Chemom. 32, e2993 https://doi.org/10.1002/cem.2993.

Laganière, J., Paré, D., Bergeron, Y., Chen, H.Y.H., Brassard, B.W., Cavard, X., 2013. Stability of soil carbon stocks varies with forest composition in the Canadian boreal biome. Ecosystems 16 (5), 852–865. https://doi.org/10.1007/s10021-013-9658-z.

Laub, M., Demyan, M.S., Nkwain, Y.F., Blagodatsky, S., Kätterer, T., Piepho, H.-P., Cadisch, G., 2020. DRIFTS peaks as measured pool size proxy to reduce parameter uncertainty of soil organic matter models. Biogeosciences 17, 1393–1413. https://doi.org/10.5194/bg-17-1393-2020.

Li, B., Morris, J., Martin, E.B., 2002. Model selection for partial least squares regression. Chemomet. Intell. Lab. Syst.ems 64 (1), 79–89. https://doi.org/10.1016/S0169-7439(02)00051-5.

Ludwig, B., Linsler, D., Höper, H., Schmidt, H., Piepho, H.-P., Vohland, M., 2016. Pitfalls in the use of middle-infrared spectroscopy: representativeness and ranking criteria for the estimation of soil properties. Geoderma 268, 165–175. https://doi.org/10.1016/j.geoderma.2016.01.010.

Luo, Y., Ahlström, A., Allison, S.D., Batjes, N.H., Brovkin, V., Carvalhais, N., Chappell, A., Ciais, P., Davidson, E.A., Finzi, A., Georgiou, K., Guenet, B., Hararuk, O., Harden, J. W., He, Y., Hopkins, F., Jiang, L., Koven, C., Jackson, R.B., Jones, C.D., Lara, M.J., Liang, J., McGuire, A.D., Parton, W., Peng, C., Randerson, J.T., Salazar, A., Sierra, C. A., Smith, M.J., Tian, H., Todd-Brown, K.E.O., Torn, M., Groenigen, K.J., Wang, Y.P., West, T.O., Wei, Y., Wieder, W.R., Xia, J., Xu, X., Xu, X., Zhou, T., 2016. Toward more realistic projections of soil carbon dynamics by Earth system models. Global Biogeochem. Cycles 30 (1), 40–56. https://doi.org/10.1002/2015GB005239.

Malhotra, A., Todd-Brown, K., Nave, L.E., Batjes, N.H., Holmquist, J.R., Hoyt, A.M., Iversen, C.M., Jackson, R.B., Lajtha, K., Lawrence, C., Vindušková, O., Wieder, W., Williams, M., Hugelius, G., Harden, J., 2019. The landscape of soil carbon data: Emerging questions, synergies and databases. Prog. Phys. Geogr.: Earth Environ. 43 (5), 707–719. https://doi.org/10.1177/0309133319873309.

Matamala, R., Calderón, F.J., Jastrow, J.D., Fan, Z., Hofmann, S.M., Michaelson, G.J., Mishra, U., Ping, C.-L., 2017. Influence of site and soil properties on the DRIFT spectra of northern cold-region soils. Geoderma 305, 80–91. https://doi.org/10.1016/j.geoderma.2017.05.014.

Matamala, R., Jastrow, J.D., Calderón, F.J., Liang, C., Fan, Z., Michaelson, G.J., Ping, C. L., 2019. Predicting the decomposability of arctic tundra soil organic matter with mid infrared spectroscopy. Soil Biol. Biochem. 129, 1–12. https://doi.org/10.1016/j.soilbio.2018.10.014.

McGuire, A.D., Anderson, L.G., Christensen, T.R., Dallimore, S., Guo, L., Hayes, D.J., Heimann, M., Lorenson, T.D., Macdonald, R.W., Roulet, N., 2009. Sensitivity of the carbon cycle in the Arctic to climate change. Ecol. Monogr. 79 (4), 523–555. https://doi.org/10.1890/08-2025.1.

Mevik, B.-H., Wehrens, R., 2007. The pls package: Principal component and partial least squares regression in R. J. Stat. Softw. 18 https://doi.org/10.18637/jss.v018.i02.

Moyano, F.E., Vasilyeva, N., Bouckaert, L., Cook, F., Craine, J., Curiel Yuste, J., Don, A., Epron, D., Formanek, P., Franzluebbers, A., Ilstedt, U., Kätterer, T., Orchard, V., Reichstein, M., Rey, A., Ruamps, L., Subke, J.-A., Thomsen, I.K., Chenu, C., 2012. The moisture response of soil heterotrophic respiration: Interaction with soil properties. Biogeosciences 9 (3), 1173–1182. https://doi.org/10.5194/bg-9-1173-201210.5194/bg-9-1173-2012-supplement.

Nocita, M., Stevens, A., Toth, G., Panagos, P., van Wesemael, B., Montanarella, L., 2014. Prediction of soil organic carbon content by diffuse reflectance spectroscopy using a local partial least square regression approach. Soil Biol. Biochem. 68, 337–347. https://doi.org/10.1016/j.soilbio.2013.10.022.

Ofiti, N.O.E., Zosso, C.U., Soong, J.L., Solly, E.F., Torn, M.S., Wiesenberg, G.L.B., Schmidt, M.W.I., 2021. Warming promotes loss of subsoil carbon through accelerated degradation of plant-derived organic matter. Soil Biol. Biochem. 156, 108185. https://doi.org/10.1016/j.soilbio.2021.108185.

Ping, C.L., Jastrow, J.D., Jorgenson, M.T., Michaelson, G.J., Shur, Y.L., 2015. Permafrost soils and carbon cycling. SOIL 1 (1), 147–171. https://doi.org/10.5194/soil-1-147-2015.

Poggio, L., de Sousa, L.M., Batjes, N.H., Heuvelink, G.B.M., Kempen, B., Ribeiro, E., Rossiter, D., 2021. SoilGrids 2.0: producing soil information for the globe with quantified spatial uncertainty. SOIL 7 (1), 217–240. https://doi.org/10.5194/soil-7-217-202110.5194/soil-7-217-2021-supplement.

R Core Team, 2021. R Studio. R Foundation for Statistical Computing. Vienna, Austria.

Ramírez, P.B., Calderón, F.J., Haddix, M., Lugato, E., Cotrufo, M.F., 2021. Using diffuse reflectance spectroscopy as a high throughput method for quantifying soil C and N and their distribution in particulate and mineral-associated organic matter fractions. Front. Environ. Sci. 9, 634472 https://doi.org/10.3389/fenvs.2021.634472.

Reeves, J.B., 2012. Mid-infrared spectral interpretation of soils: Is it practical or accurate? Geoderma 189-190, 508–513. https://doi.org/10.1016/j.geoderma.2012.06.008.

Rumpel, C., Kögel-Knabner, I., 2011. Deep soil organic matter-a key but poorly understood component of terrestrial C cycle. Plant Soil 338 (1-2), 143–158. https://doi.org/10.1007/s11104-010-0391-5.

Sanderman, J., Baldock, J.A., Dangal, S.R.S., Ludwig, S., Potter, S., Rivard, C., Savage, K., 2021. Soil organic carbon fractions in the Great Plains of the United States: an application of mid-infrared spectroscopy. Biogeochemistry 156 (1), 97–114. https://doi.org/10.1007/s10533-021-00755-1.

Sanderman, J., Savage, K., Dangal, S.R.S., 2020. Mid-infrared spectroscopy for prediction of soil health indicators in the United States. Soil Sci. Soc. Am. J. 84 (1), 251–261. https://doi.org/10.1002/saj2.20009.

Schädel, C., Bader, M.-F., Schuur, E.A.G., Biasi, C., Bracho, R., Čapek, P., De Baets, S., Diáková, K., Ernakovich, J., Estop-Aragones, C., Graham, D.E., Hartley, I.P., Iversen, C.M., Kane, E., Knoblauch, C., Lupascu, M., Martikainen, P.J., Natali, S.M., Norby, R.J., O'Donnell, J., Chowdhury, T.R., Šantrůčková, H., Shaver, G., Sloan, V., Treat, C.C., Turetsky, M.R., Waldrop, M.P., Wickland, K.P., 2016. Potential carbon emissions dominated by carbon dioxide from thawed permafrost soils. Nature Clim. Change 6 (10), 950–953. https://doi.org/10.1038/nclimate3054.

Schirrmeister, L., Froese, D., Tumskoy, V., Grosse, G., Wetterich, S., 2013. Yedoma: Late pleistocene ice-rich syngenetic permafrost of beringia, in: Encyclopedia of Quaternary Science. Elsevier, pp. 542–552. Doi: 10.1016/B978-0-444-53643-3.00106-0.

Schuur, E.A.G., McGuire, A.D., Schädel, C., Grosse, G., Harden, J.W., Hayes, D.J., Hugelius, G., Koven, C.D., Kuhry, P., Lawrence, D.M., Natali, S.M., Olefeldt, D., Romanovsky, V.E., Schaefer, K., Turetsky, M.R., Treat, C.C., Vonk, J.E., 2015. Climate change and the permafrost carbon feedback. Nature 520 (7546), 171–179. https://doi.org/10.1038/nature14338.

Shaw, C., Hilger, A., Filiatrault, M., Kurz, W., 2018. A Canadian upland forest soil profile and carbon stocks database. Ecology 99 (4). https://doi.org/10.1002/ecy.2159.

Shaw, C.H., Banfield, E., Kurz, W.A., 2008. Stratifying soils into pedogenically similar categories for modeling forest soil carbon. Can. J. Soil Sci. 88 (4), 501–516. https://doi.org/10.4141/CJSS07099.

Shu, S., Jain, A.K., Koven, C.D., Mishra, U., 2020. Estimation of permafrost SOC stock and turnover time using a land surface model with vertical heterogeneity of permafrost soils. Global Biogeochem. Cycles 34 (11). https://doi.org/10.1029/2020GB006585.

Smith, D.G., 1994. Glacial lake McConnell: Paleogeography, age, duration, and associated river deltas, Mackenzie river basin, western Canada. Quat. Sci. Rev. 13 (9-10), 829–843. https://doi.org/10.1016/0277-3791(94)90004-3.

Solly, E.F., Weber, V., Zimmermann, S., Walthert, L., Hagedorn, F., Schmidt, M.W.I., 2020. A critical evaluation of the relationship between the effective cation exchange capacity and soil organic carbon content in Swiss forest soils. Front. For. Global Change 3, 98. https://doi.org/10.3389/ffgc.2020.00098.

Soucémarianadin, L., Cécillon, L., Chenu, C., Baudin, F., Nicolas, M., Girardin, C., Delahaie, A., Barré, P., 2019. Heterogeneity of the chemical composition and thermal stability of particulate organic matter in French forest soils. Geoderma 342, 65–74. https://doi.org/10.1016/j.geoderma.2019.02.008.

Strauss, J., Schirrmeister, L., Grosse, G., Fortier, D., Hugelius, G., Knoblauch, C., Romanovsky, V., Schädel, C., Schneider von Deimling, T., Schuur, E.A.G., Shmelev, D., Ulrich, M., Veremeeva, A., 2017. Deep Yedoma permafrost: A synthesis of depositional characteristics and carbon vulnerability. Earth Sci. Rev. 172, 75–86. https://doi.org/10.1016/j.earscirev.2017.07.007.

Tarnocai, C., Bockheim, J., 2011. Cryosolic soils of Canada: Genesis, distribution, and classification. Can. J. Soil Sci. 91 (5), 749–762. https://doi.org/10.4141/cjss10020.

Tarnocai, C., Canadell, J.G., Schuur, E.A.G., Kuhry, P., Mazhitova, G., Zimov, S., Tarnocai, C., Canadell, J.G., Schuur, E.A.G., Kuhry, P., Mazhitova, G., Zimov, S., 2009. Soil organic carbon pools in the northern circumpolar permafrost region. Global Biogeochem. Cycles 23, GB2023. https://doi.org/10.1029/2008GB003327.

Tinti, A., Tugnoli, V., Bonora, S., Francioso, O., 2015. Recent applications of vibrational mid-Infrared (IR) spectroscopy for studying soil components: a review. J. Central Euro. Agric. 16, 1–22. https://doi.org/10.5513/JCEA01/16.1.1535.

Turetsky, M.R., Abbott, B.W., Jones, M.C., Anthony, K.W., Olefeldt, D., Schuur, E.A.G., Grosse, G., Kuhry, P., Hugelius, G., Koven, C., Lawrence, D.M., Gibson, C., Sannel, A. B.K., McGuire, A.D., 2020. Carbon release through abrupt permafrost thaw. Nat. Geosci. 13 (2), 138–143. https://doi.org/10.1038/s41561-019-0526-0.

Walker, D.A., Epstein, H.E., Gould, W.A., Kelley, A.M., Kade, A.N., Knudson, J.A., Krantz, W.B., Michaelson, G., Peterson, R.A., Ping, C.-L., Raynolds, M.K., Romanovsky, V.E., Shur, Y., 2004. Frost-boil ecosystems: complex interactions between landforms, soils, vegetation and climate. Permafrost Periglac. Process. 15 (2), 171–188. https://doi.org/10.1002/ppp.487.

Walker, X.J., Baltzer, J.L., Cumming, S.G., Day, N.J., Johnstone, J.F., Rogers, B.M., Solvik, K., Turetsky, M.R., Mack, M.C., 2018. Soil organic layer combustion in boreal black spruce and jack pine stands of the Northwest Territories, Canada. Int. J. Wildland Fire 27, 125–134. https://doi.org/10.1071/WF17095.

Walthert, L., Graf, U., Kammer, A., Luster, J., Pezzotta, D., Zimmermann, S., Hagedorn, F., 2010. Determination of organic and inorganic carbon, δ 13 C, and nitrogen in soils containing carbonates after acid fumigation with HCl. J. Plant Nutr. Soil Sci. 173 (2), 207–216. https://doi.org/10.1002/jpln.200900158.

Yeasmin, S., Singh, B., Johnston, C.T., Sparks, D.L., 2017. Organic carbon characteristics in density fractions of soils with contrasting mineralogies. Geochim. Cosmochim. Acta 218, 215–236. https://doi.org/10.1016/j.gca.2017.09.007.

Zimov, S.A., Schuur, E.A.G., Chapin, F.S., 2006. Permafrost and the global carbon budget. Science 312 (5780), 1612–1613.